





Article

Detecting Coastal Wetland Degradation by Combining Remote Sensing and Hydrologic Modeling

Keqi He ¹, Yu Zhang ², Wenhong Li ^{1,*}, Ge Sun ³ and Steve McNulty ³

¹ Earth and Climate Sciences, Nicholas School of the Environment, Duke University, Durham, NC 27708, USA; keqi.he@duke.edu

² Earth and Environmental Sciences Division, Los Alamos National Laboratory, Los Alamos, NM 87545, USA; yuzhang@lanl.gov

³ Eastern Forest Environmental Threat Assessment Center, USDA Forest Service Southern Research Station, USDA Forest Service, Research Triangle Park, Raleigh, NC 27709, USA; ge.sun@usda.gov (G.S.); steven.mcnulty@usda.gov (S.M.)

* Correspondence: wenhong.li@duke.edu

Abstract: Sea-level rise and climate change stresses pose increasing threats to coastal wetlands that are vital to wildlife habitats, carbon sequestration, water supply, and other ecosystem services with global significance. However, existing studies are limited in individual sites, and large-scale mapping of coastal wetland degradation patterns over a long period is rare. Our study developed a new framework to detect spatial and temporal patterns of coastal wetland degradation by analyzing fine-scale, long-term remotely sensed Normalized Difference Vegetation Index (NDVI) data. Then, this framework was tested to track the degradation of coastal wetlands at the Alligator River National Wildlife Refuge (ARNWR) in North Carolina, United States, during the period from 1995 to 2019. We identified six types of coastal wetland degradation in the study area. Most of the detected degradation was located within 2 km from the shoreline and occurred in the past five years. Further, we used a state-of-the-art coastal hydrologic model, PIHM-Wetland, to investigate key hydrologic processes/variables that control the coastal wetland degradation. The temporal and spatial distributions of simulated coastal flooding and saltwater intrusion confirmed the location and timing of wetland degradation detected by remote sensing. The combined method also quantified the possible critical thresholds of water tables for wetland degradation. The remote sensing–hydrologic model integrated scheme proposed in this study provides a new tool for detecting and understanding coastal wetland degradation mechanisms. Our study approach can also be extended to other coastal wetland regions to understand how climate change and sea-level rise impact wetland transformations.

Keywords: coastal wetland degradation; remote sensing; NDVI; climate change; sea-level rise; saltwater intrusion; hydrologic model; Alligator River National Wildlife Refuge; USA



Citation: He, K.; Zhang, Y.; Li, W.; Sun, G.; McNulty, S. Detecting Coastal Wetland Degradation by Combining Remote Sensing and Hydrologic Modeling. *Forests* **2022**, *13*, 411. <https://doi.org/10.3390/f13030411>

Academic Editor: Victor H. Rivera-Monroy

Received: 13 February 2022

Accepted: 2 March 2022

Published: 3 March 2022

Publisher's Note: MDPI stays neutral with regard to jurisdictional claims in published maps and institutional affiliations.



Copyright: © 2022 by the authors. Licensee MDPI, Basel, Switzerland. This article is an open access article distributed under the terms and conditions of the Creative Commons Attribution (CC BY) license (<https://creativecommons.org/licenses/by/4.0/>).

1. Introduction

Coastal wetlands provide critical ecological functions and services for coastal communities, such as clean water and blue carbon storage, soil erosion mitigation, biodiversity conservation, and wildlife habitat provision. Despite their importance, coastal wetlands represent the most endangered ecosystems under a warming climate [1]. The combined effects of global warming, changes in rainfall patterns, frequent extreme weather events, and sea-level rise (SLR) are significant causes of coastal wetland degradation. Through altering hydrologic processes, these disturbances dramatically affect coastal wetland structure, productivity, and ecological functions [2–11]. For example, Bianchette et al. [12] found that massive wetland tree mortality is associated with flooding from storm surges along Alabama's Gulf Coast. Hopfensperger et al. [13] showed that drought-induced saltwater intrusions sped coastal wetland deterioration rates in the Mississippi River Deltaic Plain. Furthermore, due to their low-lying nature, coastal wetlands are exceptionally

vulnerable to SLR besides more frequent floods and droughts [14,15]. Landward saltwater migration driven by SLR can significantly impact the survival and productivity of freshwater-dependent coastal plants [7].

Wetland degradation refers to the loss of wetland areas or downgrading wetland types from which the system cannot recover. It leads to a long-term reduction in vegetation coverage and changes in dominant vegetation species [16], which includes the complete loss of wetlands (change to non-wetlands), as well as the conversion of a relatively structurally complex and multi-layered wetland type (e.g., forested wetlands) to a less complex and functional wetland type (e.g., emergent herbaceous wetlands) [17–19]. “Ghost forests”, as a type of wetland degradation characterized by dead trees, falling trunks, and stumps, have emerged sporadically along the North Atlantic Coast and the Gulf of Mexico in recent decades [19,20]. However, the spatial and temporal patterns of coastal wetland degradation at a large scale have not been systematically investigated. A lack of such knowledge hinders formulating appropriate policies and implementing priorities of coastal wetland restoration [21–23].

There are two types of methods for identifying coastal wetland degradation. The first category compares observed wetland key variables (e.g., dominant plant species, hydrologic conditions, and soil organic carbon content) with their previous conditions or with nearby reference non-degraded wetlands [24–27]. Degraded coastal wetlands usually have few heterogeneous biotas [25,27,28], less suitable hydrologic conditions for wetland maintenance [9,29], and more rapid organic carbon decomposition rates [24,30]. For example, Keim et al. [29] found that the exacerbated subsidence and increased flooding reduced the productivity and regeneration of coastal wetland forests. Uzarski et al. [31] developed standardized methods and indicators to assess wetland health based on field-sampled birds, anurans, fish, macro-invertebrates, vegetation, and physicochemical conditions. These field methods can accurately distinguish degraded wetlands from healthy wetlands. However, these methods are often laborious and, thus, are costly and inapplicable to long-term and/or large-scale spatial analysis.

The other category of wetland degradation detection methods takes advantage of remote sensing technologies. This type of method [19,32,33] first trained supervised machine learning algorithms to establish the relationships between the spectral characteristics of satellite images and wetland vegetation types observed on sites. Based on the established relationships and spectral information on the remote sensing images, coastal wetland vegetation types can be estimated where field observations are lacking. Degradation locations can thus be identified from the changes of specific vegetation types during several time slices. For example, Smart et al. [19] mapped coastal wetland forests, transition-ghost forests, and marshes across the Albemarle-Pamlico Peninsula using the random forest algorithm trained by remotely sensed surface reflectance data from Landsat and LiDAR as well as 98 field observations in 2001 and 2014, respectively. Wetland vegetation types were delineated by comparing coastal vegetation classification maps over the two years. The advantages of remote sensing include collecting surface information over large spatial areas, observing coastal wetlands systematically, and monitoring their changes over time [34–36]. Unfortunately, the accuracy of the trained models for identifying vegetation types could not be assured due to a limited number of ground truths as labels for training supervised machine learning algorithms. Furthermore, the lack of sufficient long-term ground observations makes this method incapable of detecting the exact time of coastal wetland degradation.

The Normalized Difference Vegetation Index (NDVI) is one of the most widely used vegetation indices in remote sensing for assessing and monitoring vegetation coverage and ecosystem vitality [37–40]. Previous studies [41–43] successfully detected vegetation changes from local to global scales by studying the evolution of NDVI over land. For example, Pereira et al. [44] distinguished degraded and non-degraded grasslands over the Brazilian Highlands by analyzing the trend of cumulative NDVI anomalies. Similarly, using trend analysis of Moderate Resolution Imaging Spectroradiometer (MODIS) NDVI

time series, Eckert et al. [45] detected land degradation and regeneration in Mongolia. However, although NDVI effectively expresses vegetation status and monitors changes in vegetation over land [44,45], little effort has been made to quantify long-term coastal ghost forest formations and wetland losses. This study proposed a new framework to systematically detect the locations and timing of coastal wetland degradation by analyzing the fine-scale, long-term NDVI time series. We applied the framework at the Alligator River National Wildlife Refuge (ARNWR) as a case study. Then, a spatially distributed hydrologic model, PIHM-Wetland [10], was adopted to evaluate the results derived from the remote sensing-based framework and further understand the interactions between wetland degradation and hydrology key to the coastal wetland degradation over the ARNWR. This study demonstrates that a remote sensing-hydrologic model integrated scheme can effectively identify coastal wetland degradation at multiple scales and improve understanding of the relationship between coastal hydrology and vegetation dynamics.

2. Materials and Methods

2.1. Study Area

The coastal wetland study area is at the southeast part of the Alligator River National Wildlife Refuge (ARNWR), located at the Albemarle-Pamlico Peninsula in Dare County, North Carolina (NC), USA (Figure 1). This area differs from the coastal areas to the north and south due to its unique lagoonal environment and geomorphic settings, including extensive low-lying plain with very gentle slopes and poorly drained soils [46]. Buffered by Outer Banks east of the study area, this lagoonal environment is free from astronomical tides but has a micro-tidal inundation regime dominated by infrequent wind tides. These features contribute to a prevalence of wetlands [47], mainly woody wetlands and emergent herbaceous wetlands, about 81% and 15% of the study area, respectively (Figure 1). The height of the vegetation ranges from 0.6 m in emergent herbaceous wetlands to up to 30 m in woody wetlands [9]. The majority of vegetation types in the woody wetlands are evergreen forests (around 50%) and mixed forests (around 40%). Typical vegetation communities in the woody wetlands include pond pine (*Pinus serotina* Michx.), loblolly pine (*Pinus taeda* L.), red bay (*Persea borbonia* (L.) Spreng.), and sweetbay magnolia (*Magnolia virginiana* L.). Tree density varies from 13 stems/ha to 177 stems/ha, with an average density of 96 stems/ha and an average diameter at breast height (DBH) of 10 cm [48,49]. The vegetation types in emergent herbaceous wetlands are marshes (around 60%) and shrubs (around 40%) [9,46], which include black needlerush (*Juncus roemerianus* Scheele), sawgrass (*Cladium*), and panic grasses (*Panicum*) (U.S. Fish & Wildlife Service, Washington, DC, USA, https://www.fws.gov/refuge/Alligator_River/ (accessed on 5 April 2021)). Mean annual precipitation of the study area was 1366 ± 57 mm (1971–2018) and mean annual temperature from 1971 to 2000 was about 16.9 °C, with the highest and lowest temperature of 26.5 °C and 6.8 °C in July and January, respectively [9,50,51].

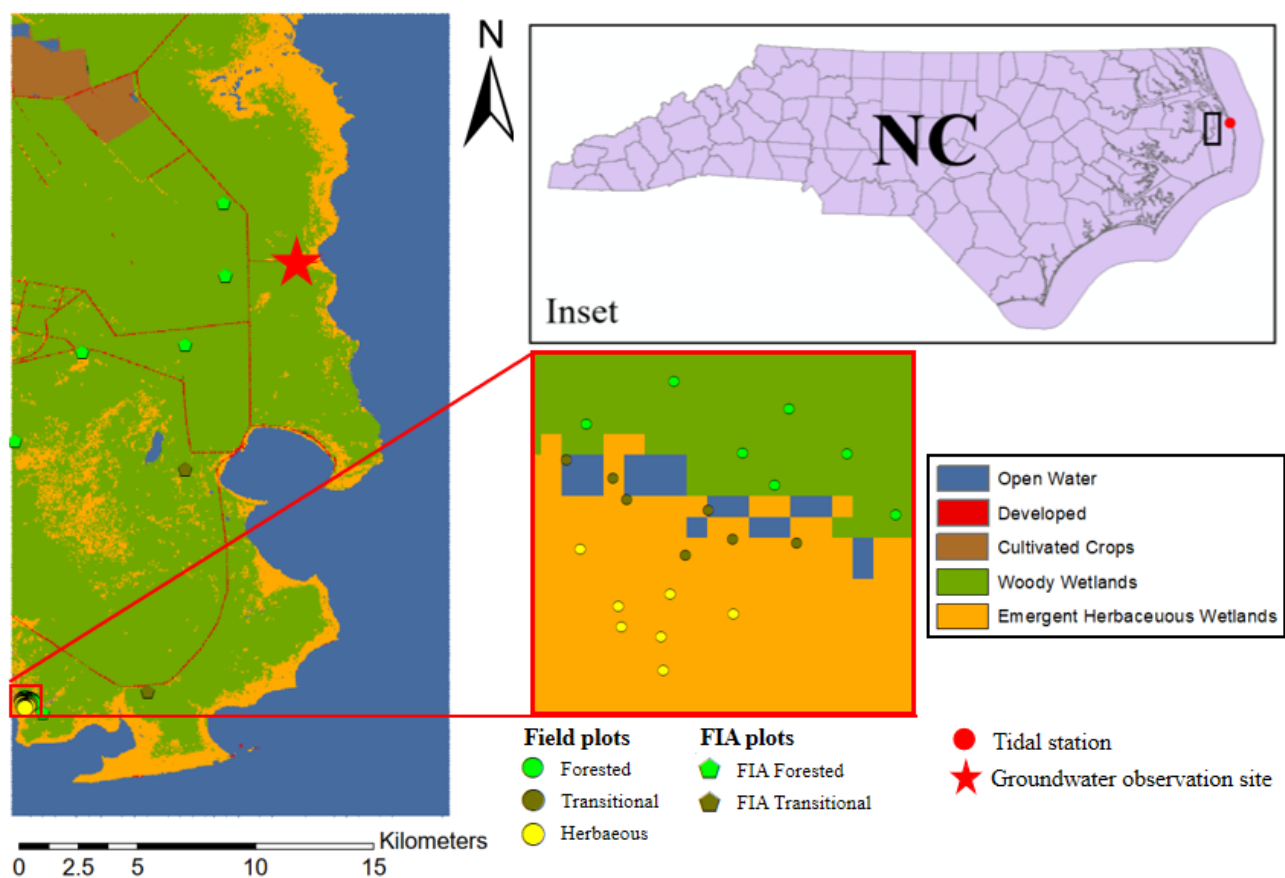


Figure 1. The study area (35.558 – 35.863° N, 75.693 – 75.859° W, excluding Open Water) with land cover types as determined by 2016 National Land Cover Database (NLCD). Inset: the location of the study area in North Carolina (NC). The black box in the inset indicates the study area. The red dot in the inset indicates the location of the NOAA tidal station (Oregon Inlet Marina, NC). The red star indicates the groundwater observation site (35.768° N, 75.750° W). The pentagon represents field plots in the Forest Inventory and Analysis (FIA) data set. The zoom-in figure in the red box shows the detailed spatial distribution of field plots obtained from Smart et al. [19], Poulter [48], and Taillie et al. [49].

The ARNWR has been experiencing rapid SLR in recent decades. For example, tidal observations at the local station Oregon Inlet Marina, NC, showed that the mean sea level has increased by 0.18 m from 1995 to 2019, with an accelerated rate since 2009 (Supplementary Figure S1). These rates are about twice as fast as eustatic SLR rates [52,53]. Moreover, the area experienced more frequent droughts and floods [14,15]. As a result, the coastal wetland ecosystems are rapidly transgressing, characterized by the conversion of wetlands to open water, mortality of low elevation forests, migration of emergent herbaceous vegetation inland, and formation of a transition zone between emergent herbaceous wetlands and forested wetlands [19,33,49].

To capture detailed information on the coastal wetland degradation, we classified the entire wetland area into three types: emergent herbaceous wetlands, transitional forested wetlands, and forested wetlands following Smart et al. [19], Poulter [48], and Taillie et al. [49]. Emergent herbaceous wetlands were defined as a mainly treeless area dominated by emergent herbaceous vegetation [46,54], whereas forested wetlands mainly consisted of living trees [55,56]. The transitional forested wetlands were the transition zones between emergent herbaceous wetlands and forested wetlands, dominated by woody vegetation with a mixture of emergent herbaceous vegetation, standing dead trees, and some persisting live trees. Thus, transitional forested wetlands and forested wetlands together consist of woody wetlands.

Except for the cultivated crop area in the northeast corner of the study area and some roads across the area (Figure 1), the study area is protected. Therefore, the area has rarely been affected by anthropogenic activities such as timber harvesting or beach development, which make the ARNWR a natural site for studying the impacts of climate change, SLR, and its associated saltwater intrusion on coastal wetland ecosystems.

2.2. Data for Wetland Degradation Detection

2.2.1. Landsat Data

To capture the details of coastal wetland degradation across the study domain, we adopted the long-term, high spatial resolution (30 m) Landsat [57,58] remote sensing data from 1995 to 2019, the same period when digitalized tidal observations are available in this study area. Due to the difference in the time coverage of different Landsat satellites, we compiled the surface reflectance products from Landsat 5 Thematic Mapper (TM), Landsat 7 Enhanced Thematic Mapper Plus (ETM+), and Landsat 8 Operational Land Imager (OLI) (courtesy of the US Geological Survey). We used 962 images (see Supplementary Section S2 for more details) with their red and near-infrared (NIR) spectral bands. All images were first processed to mask out clouds and cloud shadows based on the bit-mapped values provided in the Landsat Collection 1 Level-1 Quality Assessment (QA) Band, then co-registered to one another with a spatial accuracy of ± 1 pixel (30 m), and finally, mosaicked and clipped by the study area boundary to form mapping units.

2.2.2. Landsat-Derived Normalized Difference Vegetation Index (NDVI)

The NDVI was calculated as the ratio of the difference between near-infrared (NIR) and red reflectance measurements to their sum [59]. The formula of NDVI is as follows:

$$\text{NDVI} = \frac{\text{NIR} - \text{Red}}{\text{NIR} + \text{Red}} \quad (1)$$

where NIR and Red stand for the near-infrared and red reflectance measurements, respectively.

2.2.3. Ancillary Datasets

Previous analysis demonstrated that different vegetation types often have different NDVI values [60–62]. Therefore, NDVI ranges of wetland vegetation types from all available peer-reviewed literature were employed to establish the connections between NDVI and vegetation types. Specifically, non-vegetated areas have very low values of NDVI (i.e., 0.1 and below) [63,64], grasslands correspond to moderate values (i.e., 0.2 to 0.3) [65,66], while high NDVI values indicate rainforests (i.e., 0.6 and above) [67–72].

To further explore and confirm the correspondence between coastal wetland vegetation types and the satellite-derived NDVI values over the ARNWR (Figure 1), we also assembled coastal wetland vegetation data published by Smart et al. [19], Poulter [48], and Taillie et al. [49] and the Forest Inventory and Analysis (FIA) spatial data [73,74] from the United States Department of Agriculture's Forest Service. Measurements by Smart et al. [19], Poulter [48], and Taillie et al. [49] provided detailed information about the three coastal wetland vegetation types over the ARNWR (green, brown, and yellow dots in Figure 1). To the best of our knowledge, these data are the only field measurement data about vegetation types within our study domain available in the peer-reviewed literature. In addition, the FIA dataset [73,74] includes the most recent inventories of forests in the ARNWR. Each FIA site provides information on forests, including species, size, the health of trees, and the total tree growth and mortality. Within the study area, eight FIA plots of forested wetlands and transitional forested wetlands (green and brown pentagons in Figure 1) were available. Each FIA plot location was fuzzed within a one-mile radius circle around the actual location to protect the integrity of the FIA sample under the Food Security Act of 1985, Public Law 99–198 Stat. 1657, 23 December 1985, Confidentiality of Information, 7 U.S.C. 2276, as amended through Public Law 106–850, 31 December 2000. Different wetland types can be distinguished by comparing the NDVI values at these field

measurement sites. Furthermore, the results are compared with land cover maps classified by the National Oceanic and Atmospheric Administration Coastal Change Analysis Program (C-CAP, with the same spatial resolution and available in 1996, 2001, 2011, and 2016) [75] to evaluate the performance of NDVI-based wetland classification.

2.3. Methodology

Figure 2 showed the workflow of the study. First, we proposed a new remote sensing-based framework to identify when and where coastal wetland degradation occurred (Section 3.1). Then, the PIHM-Wetland model was employed to simulate hydrologic variables, including groundwater tables (GWTs) and saltwater tables (SWTs), key to coastal wetland degradation. Lastly, we investigated the mechanism of coastal wetland degradation by analyzing simulated GWTs and SWTs at the locations that degradation occurred.

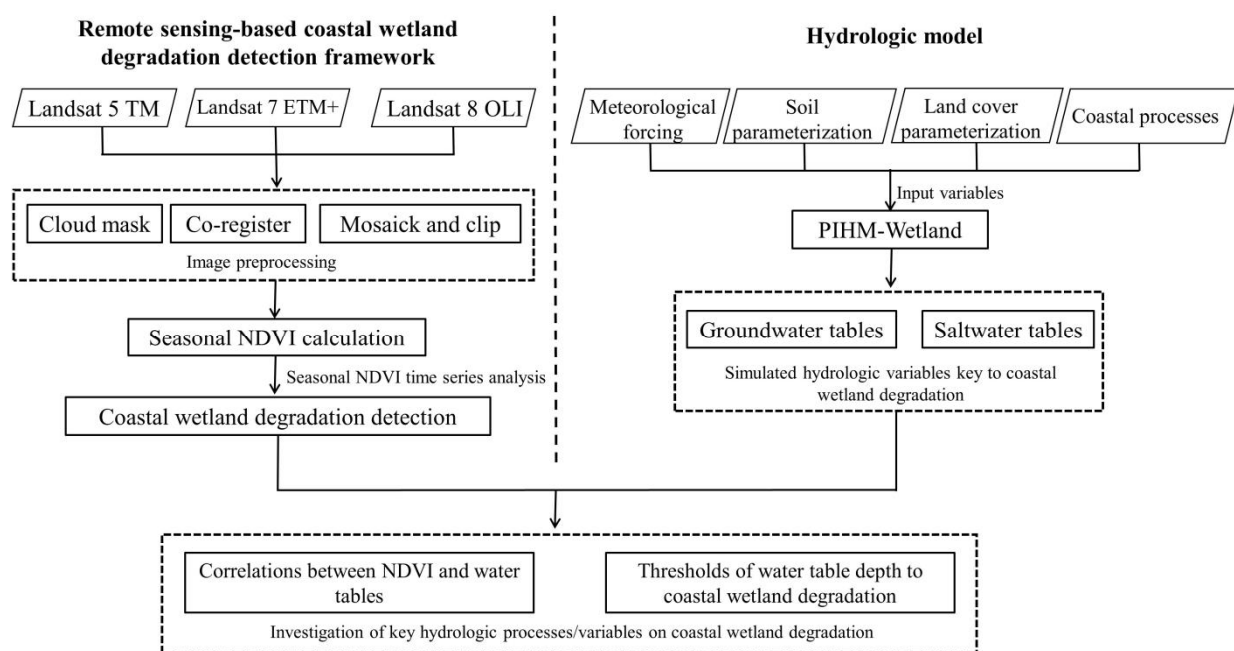


Figure 2. The workflow of this study.

2.3.1. PIHM-Wetland Model

Previous research demonstrated that disturbances/drivers affect wetlands degradation mainly through altering their hydrologic processes [3,4,6–10]. Therefore, to evaluate the results obtained from the coastal wetland degradation detection framework and understand the causes of degraded wetlands from hydrologic aspects, a coastal wetland hydrologic model, PIHM-Wetland [10], was employed over the ARNWR. The PIHM-Wetland model is a distributed, physically based, and coastal processes coupled hydrologic model [10]. It tracks the changes of the groundwater, soil water, and saltwater by simulating water exchange through canopy interception, infiltration, overland flow, channel flow, unsaturated and saturated water flow, saltwater lateral flow, and evapotranspiration (ET). The model has been successfully employed to study the wetland resilience of this study area [9,10].

2.3.2. Data Used in the PIHM-Wetland Model

PIHM-Wetland uses openly available national datasets for meteorological forcing, soil parameterizations, land cover properties, and coastal processes. Specifically, we used meteorological data from Phase 2 of the National Land Data Assimilation System (NLDAS-2) [76] as the forcing data, including precipitation, surface air temperature, specific humidity, air pressure, and solar radiation due to their agreement with the in-situ measurements from the observation sites [10]. For soil parameterizations, the national Gridded Soil Survey

Geographic database (gSSURGO) was utilized to derive vertical and horizontal hydraulic conductivity, porosity, and coefficients for the soil–water retention curve to simulate the infiltration processes, recharge, and lateral groundwater flow. Finally, for land cover properties that govern the processes of ET, overland flow, and energy budget, the Mapped Monthly Vegetation Data (<https://ldas.gsfc.nasa.gov/nldas/web/web.veg.monthly.table.html> (accessed on 9 November 2020)) was applied to obtain maximum leaf area index (LAI), minimum stomatal resistance, reference stomatal resistance, albedo, vegetation fraction, Manning’s roughness, and root zone depth. Moreover, we adopted the tide observations from the nearest National Oceanic and Atmospheric Administration (NOAA) tidal station (Oregon Inlet Marina, NC, Figure 1) (<https://tidesandcurrents.noaa.gov/> (accessed on 13 November 2020)) in the coastal process simulation. Detailed descriptions and formulations of the PIHM-Wetland model can be found in Zhang et al. [10]. Besides, Digital Elevation Model (DEM) from the US Geological Survey (USGS) was employed to generate PIHM-Wetland unstructured triangular grids.

2.3.3. Model Setup

The entire study area was decomposed into 17459 unstructured triangular elements based on the domain topography, with an average size (longest edge of the triangular element) around 100 m. The boundary at the ocean–land interface was set as an open boundary condition, where terrestrial surface and subsurface water interact with coastal sea-level changes. In contrast, the inland boundary was set as a closed boundary condition. Moreover, the soil layer of each element was divided into two layers: a well-drained top layer (0–0.3 m) and a poorly drained bottom layer (0.3–1 m) according to the soil features obtained from the gSSURGO dataset and field measurements [9,10]. Groundwater table observations showed that the subsurface hydrologic activities primarily occur in the top one-meter soil zone [51].

The PIHM-Wetland model was first calibrated and validated by comparing the simulated GWT and ET with in-situ GWTs (Figure 1) and MODIS ET. Next, model performance was evaluated by Nash-Sutcliffe Efficient (NSE, [77]) (see [10]). Then, a 25-year hydrologic simulation from 1995 to 2019 with daily outputs was conducted after a ten-year spinning-up (the system reached a relative equilibrium state). Finally, as the water level has critical impacts on coastal wetlands’ health and survival [9,13,78,79], we analyzed GWTs and SWTs from the model simulation to assess the wetland hydrologic resilience to climate change [4,9,10]. In this study, negative (positive) water tables represent the water level below (above) ground.

3. Results and Discussion

3.1. Framework to Detect Wetland Degradation

We proposed a new framework by analyzing seasonal NDVI time series to identify when and where coastal wetland degradation occurred. As Landsat crosses every point on Earth once every 16 days, a maximum of two images are available in a month. However, many monthly scale NDVI data contain missing values due to clouds and aerosols over the study area. Annual scale NDVI can minimize cloud contamination issues, but it smoothed out the seasonal vegetation variations and reduced the data available for analysis. Thus, seasonal scale NDVI data were used. This study obtained the seasonal NDVI value as the maximum of all available NDVI in the same season instead of the average value. We used the maximum rather than the average value to avoid the potential issues of broken and thin clouds, which may not be adequately masked out and would slightly reduce the value of NDVI [80,81]. It turned out that the seasonal NDVI time series allowed us to not only get NDVI values almost without contamination from clouds and aerosols at each pixel in the study area but also more accurately capture canopy transitions in the coastal wetland ecosystems. Here, the four seasons are defined as spring (March–May, MAM), summer (June–August, JJA), fall (September–November, SON), and winter (December of the current year and January and February of the following year, DJF), respectively. We

analyzed the seasonal NDVI time series during the period from 1995 to 2019 to determine where and when coastal wetlands degraded in each pixel based on the established criteria described below.

We first analyzed field-collected wetland plots from Smart et al. [19], Poulter [48], Tailie et al. [49], FIA dataset [73,74], and their corresponding maximum seasonal NDVI values in the collection years to explore and confirm the correspondence between coastal wetland vegetation types and the satellite-derived NDVI values over the ARNWR (Figure 3). Emergent herbaceous wetlands and non-vegetated areas are well separated from forested and transitional forested wetlands. The NDVI values of the forested wetlands are significantly higher compared to those of the transitional forested wetlands (Figure 3), in agreement with the conclusion of Anyamba and Tucker [65], Bhandari et al. [67], Chouhan and Sarma [68], Gandhi et al. [69], Jamali et al. [63], Karlsen et al. [64], Meneses-Tovar [70], Rousta et al. [71], Weier and Herring [72], and Zheng et al. [66]. Table 1 summarized the NDVI ranges for different coastal wetland types: for forested wetlands, its maximum seasonal NDVI values within a year fall in 0.5 to 1.0; for transitional forested wetlands, the range is 0.4 to 0.5; for emergent herbaceous wetlands, the range is 0.1 to 0.4; and when the seasonal NDVI values within a year are all smaller than 0.1, the area is considered as non-vegetated areas. According to these NDVI-based criteria, our coastal wetland classification results are consistent with the classification in C-CAP, confirming the feasibility and accuracy of using NDVI ranges to classify coastal wetlands into forested wetlands, transitional forested wetlands, and emergent herbaceous wetlands.

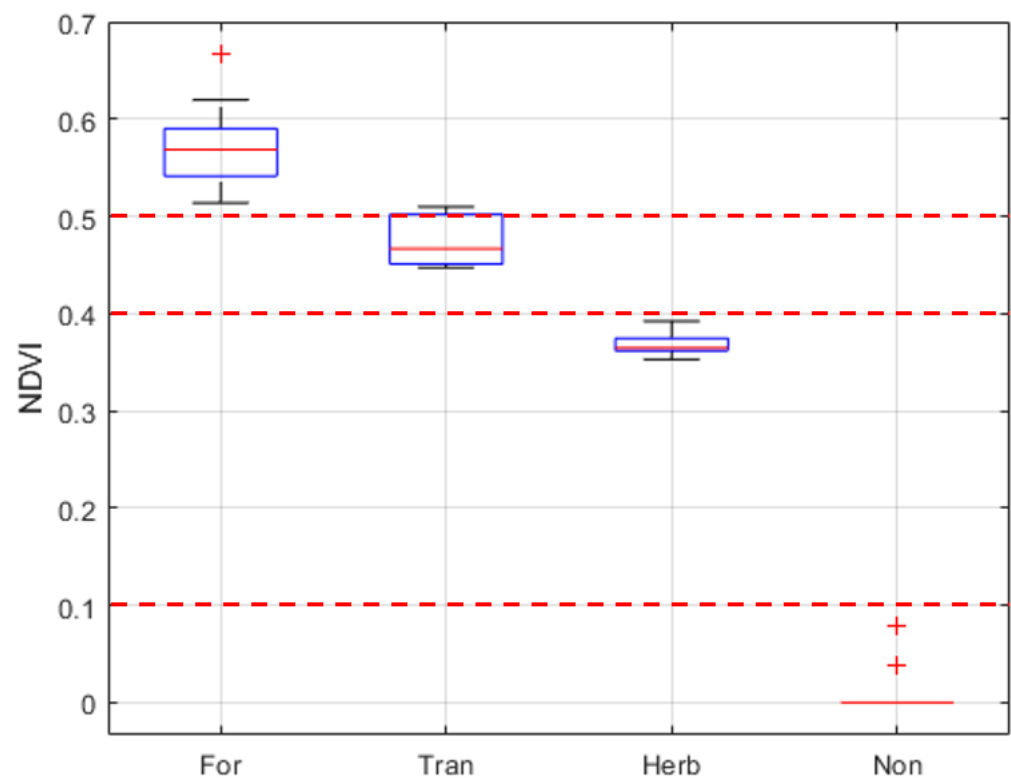


Figure 3. Box plots of NDVI for forested wetlands (For), transitional forested wetlands (Tran), emergent herbaceous wetlands (Herb), and non-vegetated areas (Non), respectively. Red horizontal dash lines represent thresholds (0.5, 0.4, 0.1) between different wetland types. The red solid horizontal line, box, and whisker ends indicate the median, 25th and 75th percentiles, and the 10th and 90th percentiles, respectively. The data points outside the ranges are shown by the red plus (+) sign.

Table 1. NDVI ranges and structural complexity of different coastal wetland types.

Coastal Wetland Types	NDVI Ranges	Structural Complexity
Forested wetlands	$0.5 \leq \text{NDVI} \leq 1.0$	Very High
Transitional forested wetlands	$0.4 \leq \text{NDVI} < 0.5$	High
Emergent herbaceous wetlands	$0.1 \leq \text{NDVI} < 0.4$	Moderate
Non-vegetated areas	$-1.0 \leq \text{NDVI} < 0.1$	Low

After establishing the correspondence between coastal wetland types and NDVI ranges, whether wetlands are degraded can be identified by analyzing NDVI and its change over time at each pixel. Figure 4 shows the entire framework of wetland degradation detection by analyzing seasonal NDVI time series. Specifically, we considered six types of wetland degradation (Table 2 and Figure 4). Forested wetlands ($0.5 \leq \text{NDVI} \leq 1.0$) could degrade to transitional forested wetlands ($0.4 \leq \text{NDVI} < 0.5$, Type 3 degradation in Table 2 and Figure 4), emergent herbaceous wetlands ($0.1 \leq \text{NDVI} < 0.4$, Type 2 degradation in Table 2 and Figure 4), or non-vegetated areas ($-1.0 \leq \text{NDVI} < 0.1$, Type 1 degradation in Table 2 and Figure 4); transitional forested wetlands ($0.4 \leq \text{NDVI} < 0.5$) could degrade to emergent herbaceous wetlands ($0.1 \leq \text{NDVI} < 0.4$, Type 5 degradation in Table 2 and Figure 4), or non-vegetated areas ($-1.0 \leq \text{NDVI} < 0.1$, Type 4 degradation in Table 2 and Figure 4); emergent herbaceous wetlands ($0.1 \leq \text{NDVI} < 0.4$) could only degrade to non-vegetated areas ($-1.0 \leq \text{NDVI} < 0.1$, Type 6 degradation in Table 2 and Figure 4). Meanwhile, the specific year when degradation occurred can be accurately determined (Supplementary Section S3).

Table 2. Identified Wetland degradation over the ARNWR from 1995–2019.

Type	Wetland Degradation Types	Number of Wetland Degradation Pixels ¹	Areas of Wetland Degradation (Hectares)	Degradation Percentage of the Study Area (%)
1	Forested wetland degraded to non-vegetated areas	930	84	0.21
2	Forested wetlands degraded to emergent herbaceous wetlands	2538	228	0.56
3	Forested wetlands degraded to transitional forested wetlands	20,011	1801	4.44
4	Transitional forested wetlands degraded to non-vegetated areas	1276	115	0.28
5	Transitional forested wetlands degraded to emergent herbaceous wetlands	10,681	961	2.37
6	Emergent herbaceous wetlands degraded to non-vegetated areas	4224	380	0.94
	Sum	39,660	3569	8.80

¹ The number of wetland degradation pixels summarized here only counts those wetlands that initially have a relatively complex structure before degrading to a relatively simple structure by the end of 2019, regardless of the intermediate types they went through. For example, for wetlands with forested wetland degrading to non-vegetated areas (Type 1 degradation), they were original forested wetlands and experienced transitional forested wetland states, then emergent herbaceous wetland states, and finally non-vegetated area states from 1995 to 2019. In this study, these wetlands were only counted as forested wetland degraded to non-vegetated areas (Type 1 degradation). Therefore, every degraded wetland pixel only belongs to a certain type of wetland degradation and is only counted once.

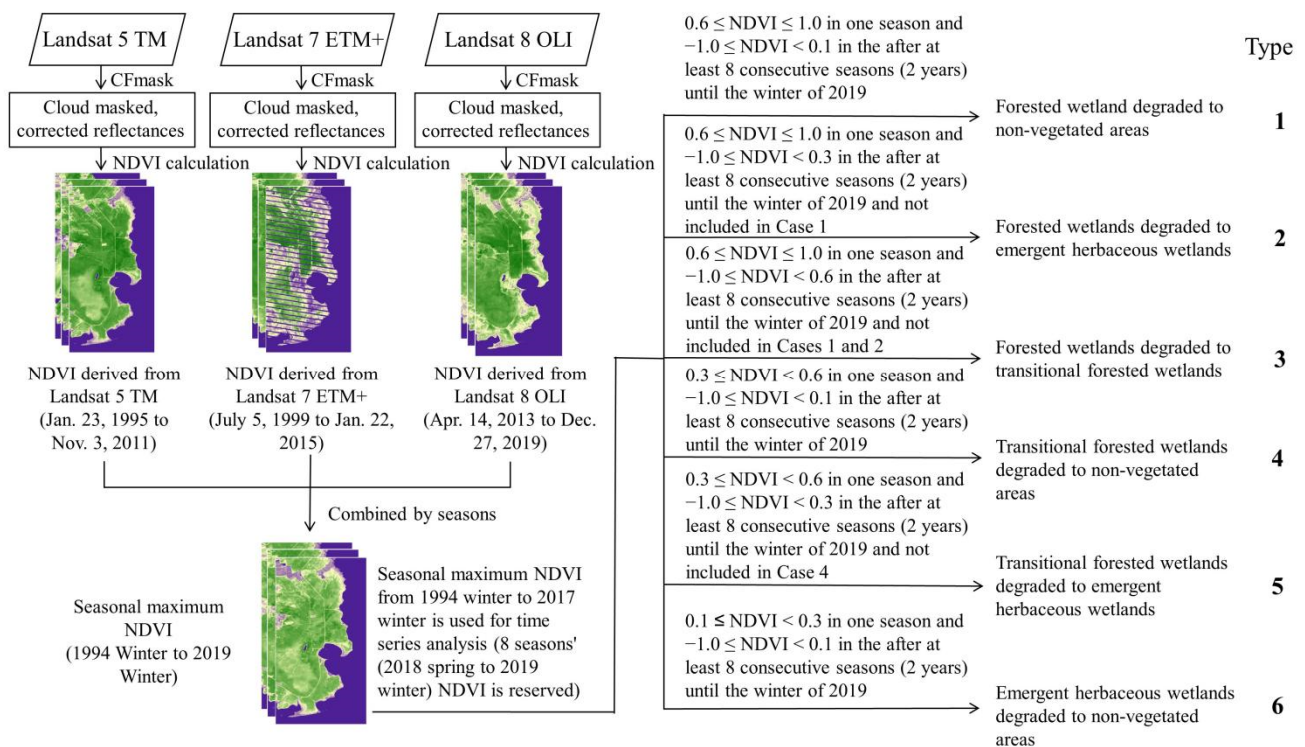


Figure 4. A framework of wetland degradation detection by analyzing seasonal NDVI time series derived from Landsat.

Here, we show an example of applying the framework to a randomly selected pixel within ARNWR from 1995 to 2019 (Figure 5). In 1995, the maximum seasonal NDVI by pixel was 0.55, suggesting that the selected wetland was forested ($0.5 \leq \text{NDVI} \leq 1.0$). However, the maximum seasonal NDVI values of the wetland pixel fell below 0.4 in 2003 and never came back to 0.5 (the lower NDVI threshold of forested wetlands) by the end of the study period (2019 winter). It indicated that the forested wetland changed to an emergent herbaceous wetland in 2003; thus, this pixel is labeled as the Type 2 wetland degradation, and the degradation occurred in 2003. We noticed that in 1996 and 2000, the maximum seasonal NDVI values were 0.42 and 0.47, respectively (Figure 5), lower than 0.5, but in the following years (1997 and 2001, respectively), the NDVI values came back to be higher than 0.5. These implied that disturbances might cause NDVI values to decrease temporarily in 1996 and 2000. However, these disturbances were still within the self-restoring capacity, and wetlands re-flourished in the year following the disturbances. Similar phenomena were also founded by Armitage et al. [82], Hu and Smith [83], and Steyer et al. [84], suggesting that if the disturbances are short-term and not beyond the wetland resilience, the vegetation can re-grow in the following growing season/year after the disturbances. Thus, for the degraded wetland pixels, their seasonal NDVI values must be continuously below the NDVI threshold of the relatively higher structure-complex wetland type for at least eight consecutive seasons until the end of the study period. Detailed criteria for different types of wetland degradation are summarized in Figure 4.

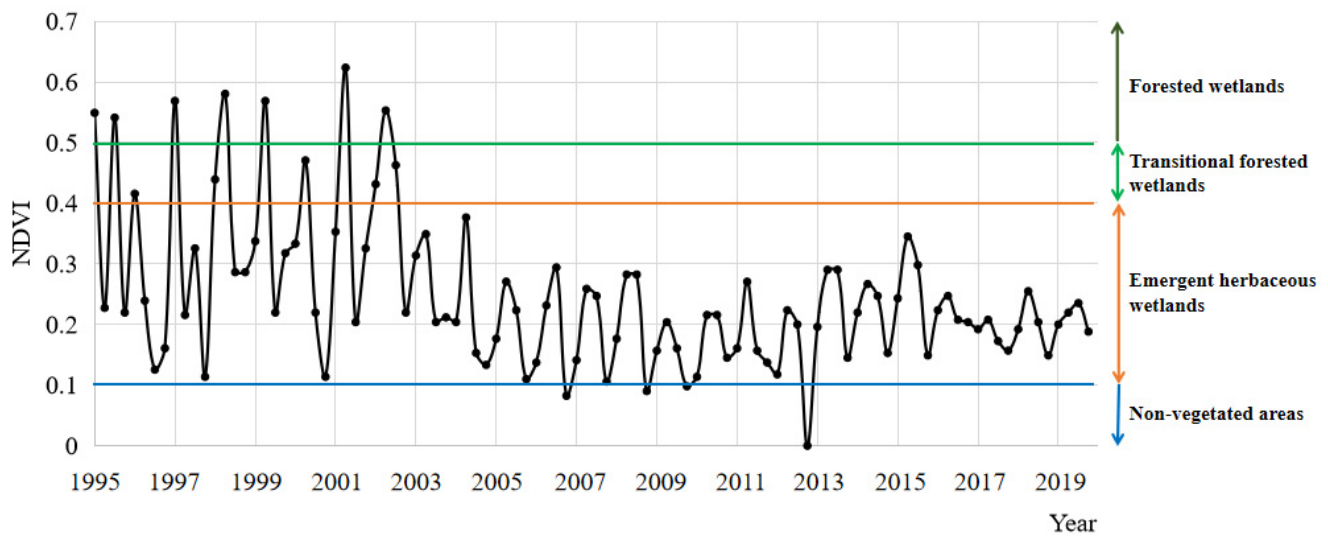


Figure 5. Evolution of seasonal NDVI values of a randomly selected pixel with the Type 2 wetland degradation within ARNWR from 1995 to 2019.

3.2. Wetland Degradation during the Period from 1995 to 2019

3.2.1. Detected Locations of Wetland Degradation over the ARNWR

We summarize the detected degradation of the coastal wetlands over the ARNWR from 1995 to 2019 (Table 2 and Figure 6). In 1995, the study domain's total wetland area, i.e., the sum of forested wetlands, transitional forested wetlands, and emergent herbaceous wetlands, was 40,542 hectares (ha). Over the 25 years, a total of 3569 ha (8.8% of the study area) of wetlands have degraded, and 579 ha (1.4% of the study area) have been de-vegetated, mostly converted to open water (Table 2). Specifically, about 84,228 and 1801 ha of forested wetlands are found to degrade to non-vegetated areas (Type 1 degradation), emergent herbaceous wetlands (Type 2 degradation), and transitional forested wetlands (Type 3 degradation), respectively. About 115 ha of transitional forested wetlands changed to non-vegetated areas (Type 4 degradation), and 961 ha changed to emergent herbaceous wetlands (Type 5 degradation). Original emergent herbaceous wetlands disappeared by 380 ha (Type 6 degradation). For those pixels that experienced more than one type of degradation during the 25-year period, for instance, original forested wetlands converted into transitional forested wetlands, then emergent herbaceous wetlands, and finally non-vegetated areas, Table 2 only counts these pixels as the Type 3 degradation for simplicity; but the framework presented here and the PIHM-Wetland model analysis are still valid for these pixels (not shown).

A net loss of 1388 ha (3.4% of the study area) of woody wetlands over the 25 years was detected (Table 2), highlighting the dire situation that woody wetlands face in a warming climate. Several studies [19,33,49] also confirmed the losses of woody wetlands in the ARNWR. On the other hand, the emergent herbaceous wetlands increased by about 213.0% during the study period; this is mainly because the conversion of woody wetlands (transitional forested wetlands plus forested wetlands) to the emergent herbaceous wetlands was more significant than the degradation of emergent herbaceous wetlands (Table 2).

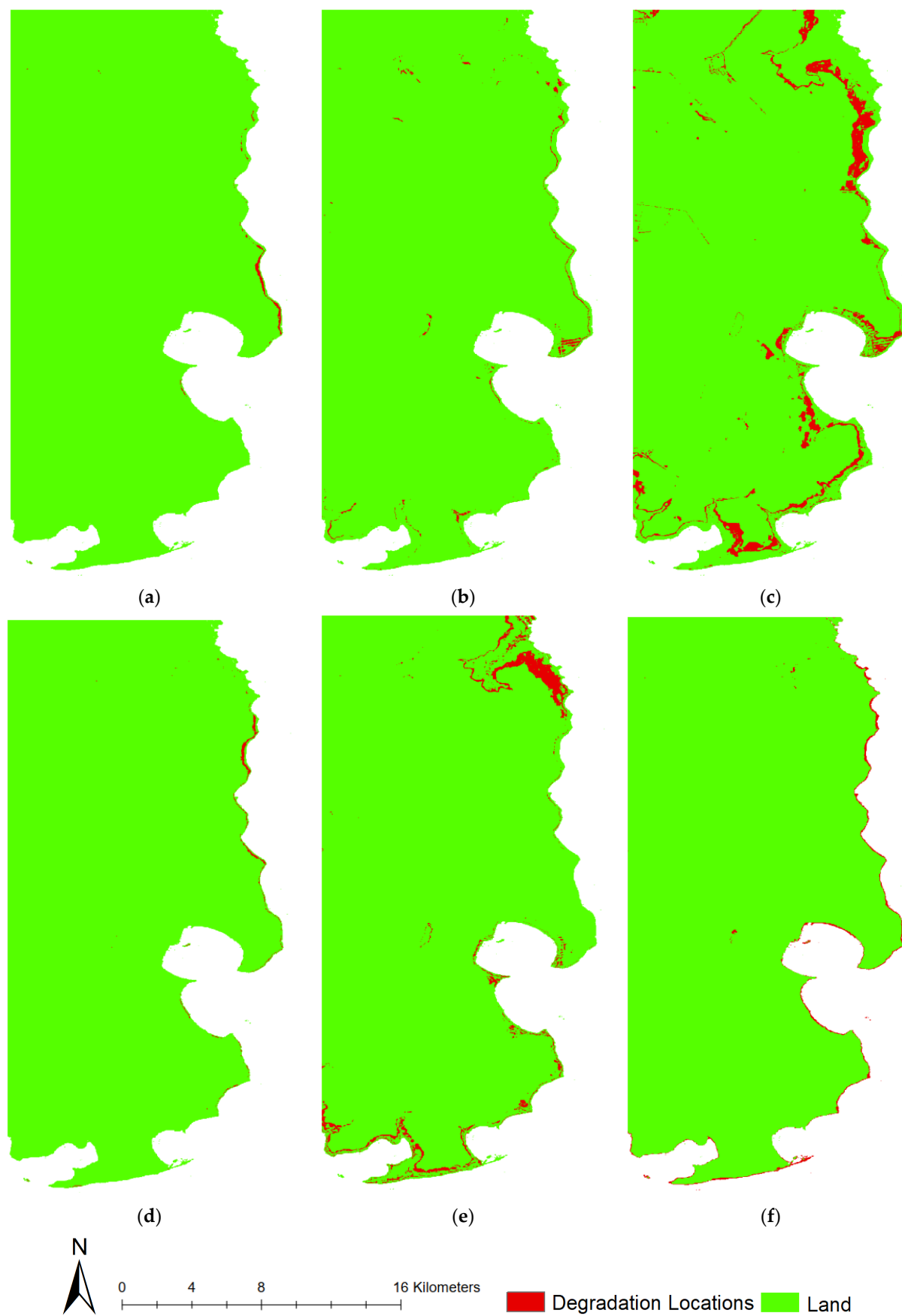


Figure 6. Detected wetland degradation locations over the ARNWR from 1995 to 2019. (a) Type 1 degradation: Forested wetlands degrading to non-vegetated areas; (b) Type 2 degradation: Forested

wetlands degrading to emergent herbaceous wetlands; (c) Type 3 degradation: Forested wetlands degrading to transitional forested wetlands; (d) Type 4 degradation: Transitional forested wetlands degrading to non-vegetated areas; (e) Type 5 degradation: Transitional forested wetlands degrading to emergent herbaceous wetlands; and (f) Type 6 degradation: Emergent herbaceous wetlands degrading to non-vegetated areas. (Red: Degradation Locations; Green: Land).

Detected wetland degradation mainly occurred within 2 km of the shoreline (Figure 6). At the same time, Type 3 (forested wetlands to transitional forested wetlands) and Type 5 (transitional forested wetlands to emergent herbaceous wetlands) degradations were also found in the interior part of the landscape or along the developed road (Figure 6c) and at the flooding plain northeast of the study area (Figure 6e), respectively. Figure 6 also indicates a gradient of the wetland degradation from the shoreline to the inland. Therefore, it is not surprising that the detected degradation was in the order of emergent herbaceous wetlands (Figure 6f), transitional forested wetlands (Figure 6d,e), and forested wetlands from the sea toward land (Figure 6a–c) given that emergent herbaceous wetlands and woody wetlands were initially distributed along with shoreline areas and inland, separately (Figure 1).

For the pixels that initially were classified as the same wetland type, the wetlands closer to the sea tended to degrade to more minor structural-complex wetland types than those further to the ocean (Figure 6). For example, for the initial forested wetlands, the Type 1 degradation (forested wetlands degrading to non-vegetated areas) occurred closest to the sea, while Type 2 (forested wetlands degrading to emergent herbaceous wetlands) and Type 3 degradations (forested wetlands degrading to transitional forested wetlands) were in more inland areas. Similar patterns can also be found for the transitional forested wetlands pixels (Figure 6d,e). This phenomenon emphasizes the impacts of rising sea levels and their associated saltwater intrusions on coastal wetland degradation.

3.2.2. Detected Time of Wetland Degradation

We also determined the time when the identified wetland degradation occurred using this framework. Figure 7 summarizes the total number of wetland pixels experiencing degradation over the ARNWR in each year. Most wetland degradation occurred within the past five years; 2014 and 2017 witnessed the most significant percentage of coastal wetland degradation.

3.2.3. Uncertainties in Detected Coastal Wetland Degradation

In this study, thresholds of NDVI for different coastal wetland types were determined through analyzing and synthesizing literature, field measurements, and FIA data. Due to the scarcity of field data, NDVI thresholds for different wetland types are only accurate to one decimal place. Thus, a change of thresholds of NDVI may lead to the change of the exact number of detected wetland degradation pixels. Nevertheless, the overall spatio-temporal patterns of coastal wetland degradation will not change (not shown). In addition, compared to the C-CAP land cover classification maps, woody wetlands classified in this study are highly consistent with forested wetlands and scrub/shrub wetlands in C-CAP (user accuracy of 95%), and emergent herbaceous wetlands classified here correspond to emergent wetlands in C-CAP (user accuracy of 62%). Thus, the wetland classification results from the proposed framework are highly consistent with those of the C-CAP Scheme, and the framework could be applied to other coastal wetland regions. For areas with long-term field observations, thresholds of NDVI values can be accurately determined for different wetland types. In contrast, several rough thresholds can be estimated based on previous studies and experts' experience for areas with almost no historical in-situ measurements or hard to access. After determining the NDVI ranges of different wetland types, wetland degradation can be detected by analyzing NDVI time series derived from free-available and global-covered Landsat data.

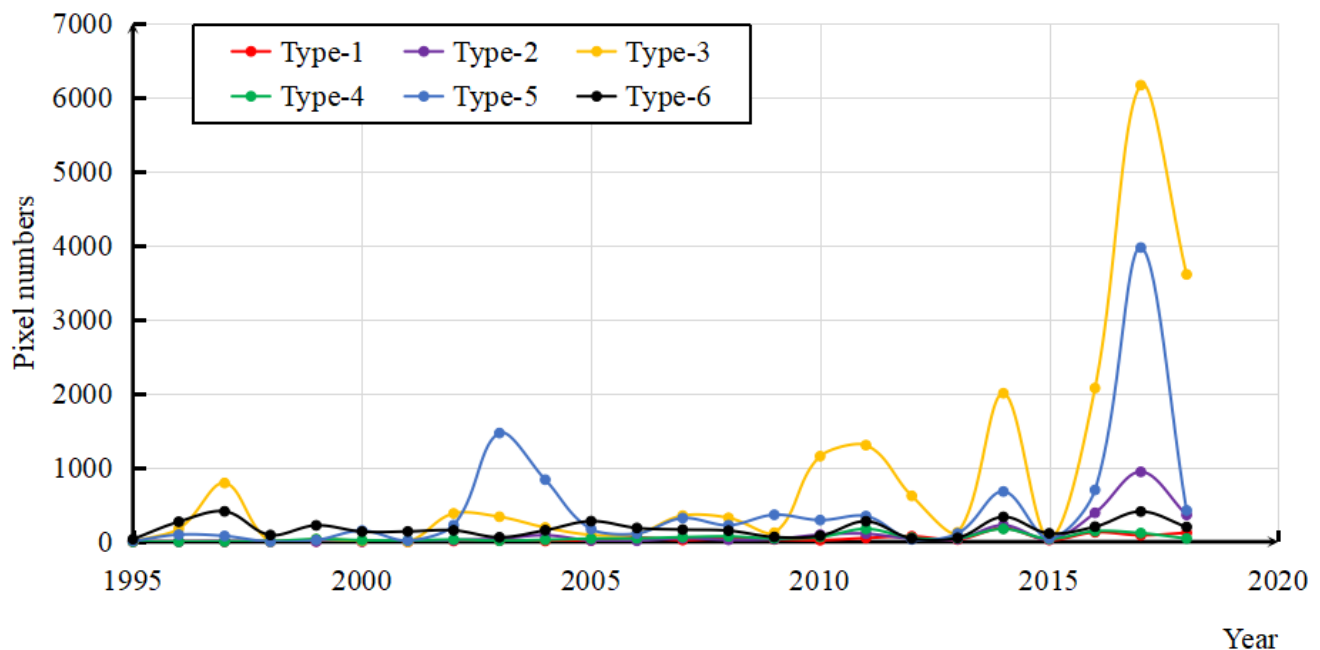


Figure 7. The number of pixels with wetland degradation in each year. Each pixel has an area of 30 m × 30 m.

Besides, multiple surface reflectance imageries from Landsat 5 TM, 7 ETM+, and 8 OLI were used in the study. The sensors carried by Landsat 5 TM and Landsat 7 ETM+ have almost the same spectral bands, while the sensor of Landsat 8 OLI has narrower bands. According to Ke et al. [85], Roy et al. [86], and Xu and Guo [87], NDVI calculated from Landsat 8 OLI images is slightly larger than that calculated from Landsat 5 TM/7 ETM+ images in lower-vegetation covered areas. As for our study, the slight difference of NDVI between Landsat 8 OLI and Landsat 5 TM/7 ETM+ can be negligible since it is considered that wetland degradation occurred when NDVI values were continuously below the NDVI threshold of the relatively higher structurally complex wetland type for eight consecutive seasons.

3.3. PIHM-Wetland Modeling Analysis

3.3.1. The Selected Transect for Analysis

To analyze hydrologic processes key to the changes of coastal wetlands, we selected model grids along a transect almost perpendicular to the shoreline (Figure 8) because emergent herbaceous wetlands, transitional forested wetlands, and forested wetlands are located from the shoreline to inland successively. The transect included five representative model grids with detected wetland degradation, i.e., emergent herbaceous wetlands degrading to non-vegetated areas (Type 6 degradation, Figure 8a), transitional forested wetlands degrading to emergent herbaceous wetlands (Type 5 degradation, Figure 8c), forested wetlands degrading to transitional forested wetlands (Type 3 degradation, Figure 8e) and model grids without wetland degradation (emergent herbaceous wetlands (Figure 8b) and transitional forested wetlands (Figure 8d)), respectively, during the period from 1995 to 2019.

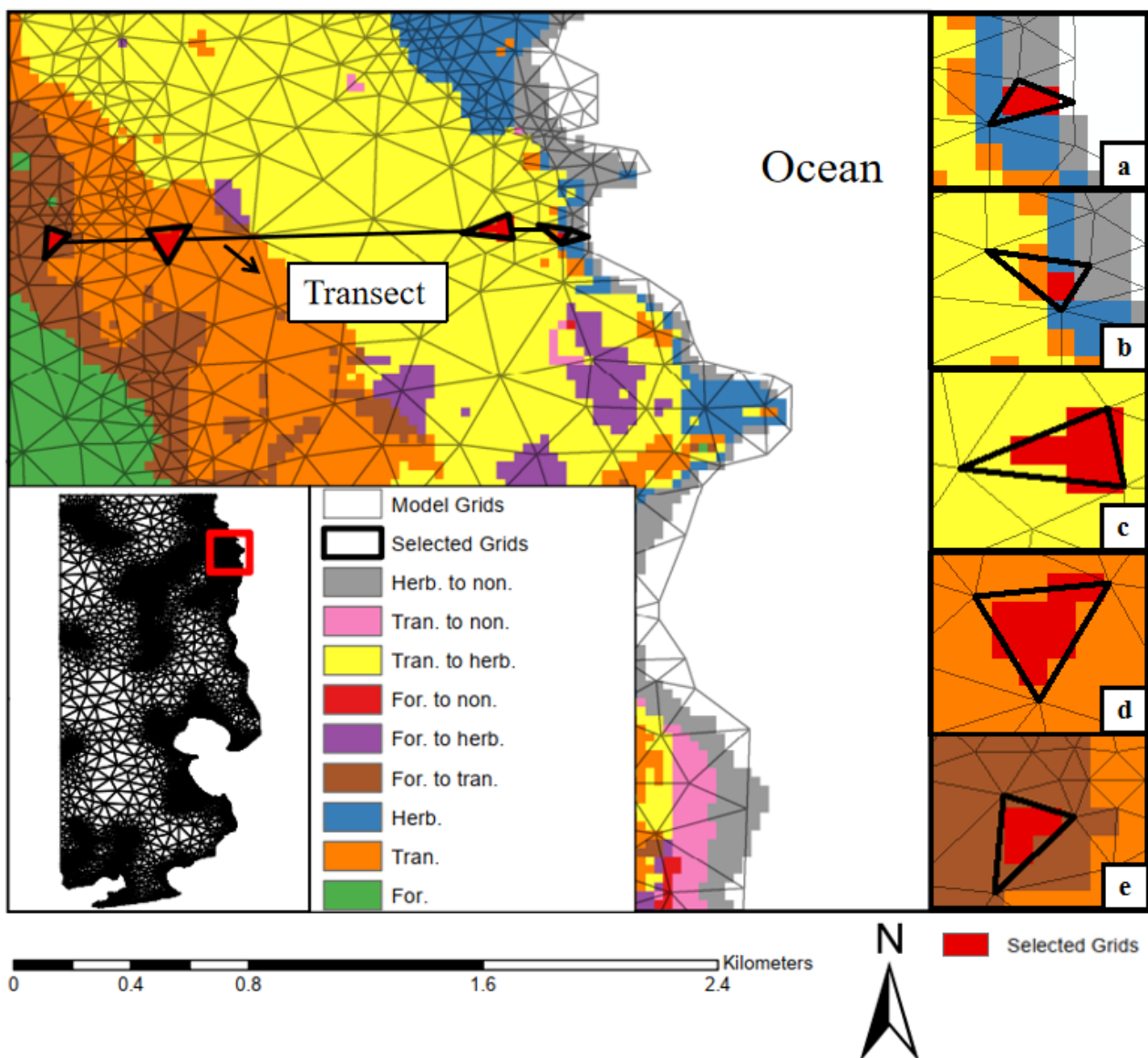


Figure 8. The selected transect and representative model triangular grids. (a) Emergent herbaceous wetlands degrading to non-vegetated areas (Type 6 degradation); (b) Emergent herbaceous wetlands without degradation; (c) Transitional forested wetlands degrading to emergent herbaceous wetlands (Type 5 degradation); (d) Transitional forested wetlands without degradation; (e) Forested wetlands degrading to transitional forested wetlands (Type 3 degradation). (For.: Forested wetlands; Tran.: Transitional forested wetlands; Herb.: Emergent herbaceous wetlands; Non.: Non-vegetated areas).

3.3.2. Correlations between NDVI and Water Tables

Firstly, we explored the relationship between annual maximum NDVI and seasonal/annual water tables to understand the impacts of water table variations on wetlands. Wetland managers and stakeholders are more interested in the degradation information on yearly scales [88,89], and seasonal-scale GWTs/SWTs could elucidate the role of water table variation/change on degradation [90–92]. In addition, the resulting figure can be much clearer without seasonal cycles, and the overall conclusions using seasonal NDVI are similar to those using annual maximum NDVI (Supplementary Section S4).

We calculated the correlations between grid-wise mean annual maximum NDVI and seasonal/annual mean GWTs and SWTs (Figure 9) for the model grids in Section 3.3.1 and Figure 8. The model grids (spatial resolution on average 100 m) may include a few Landsat pixels (30 m × 30 m). Still, we chose the pixels that have the same type of

wetland degradation/non-degradation with similar NDVI values within the model grids and averaged the vegetation indexes at these pixels to get the grid-wise mean NDVI values. It is shown that NDVI was negatively correlated with GWTs and SWTs for all the grids with coastal wetland degradation (Figure 9a,c,e) but positively correlated with GWTs and SWTs for the grids where coastal wetlands did not degrade (Figure 9b,d). For the grids with wetland degradation, the negative correlations between NDVI and SWTs were more robust than those between NDVI and GWTs, especially in the summer season. These features are much more apparent for Type 6 and Type 5 degradations (Figure 9a,c). Their correlations between NDVI and summer SWTs are -0.53 and -0.68 (p values < 0.01), respectively.

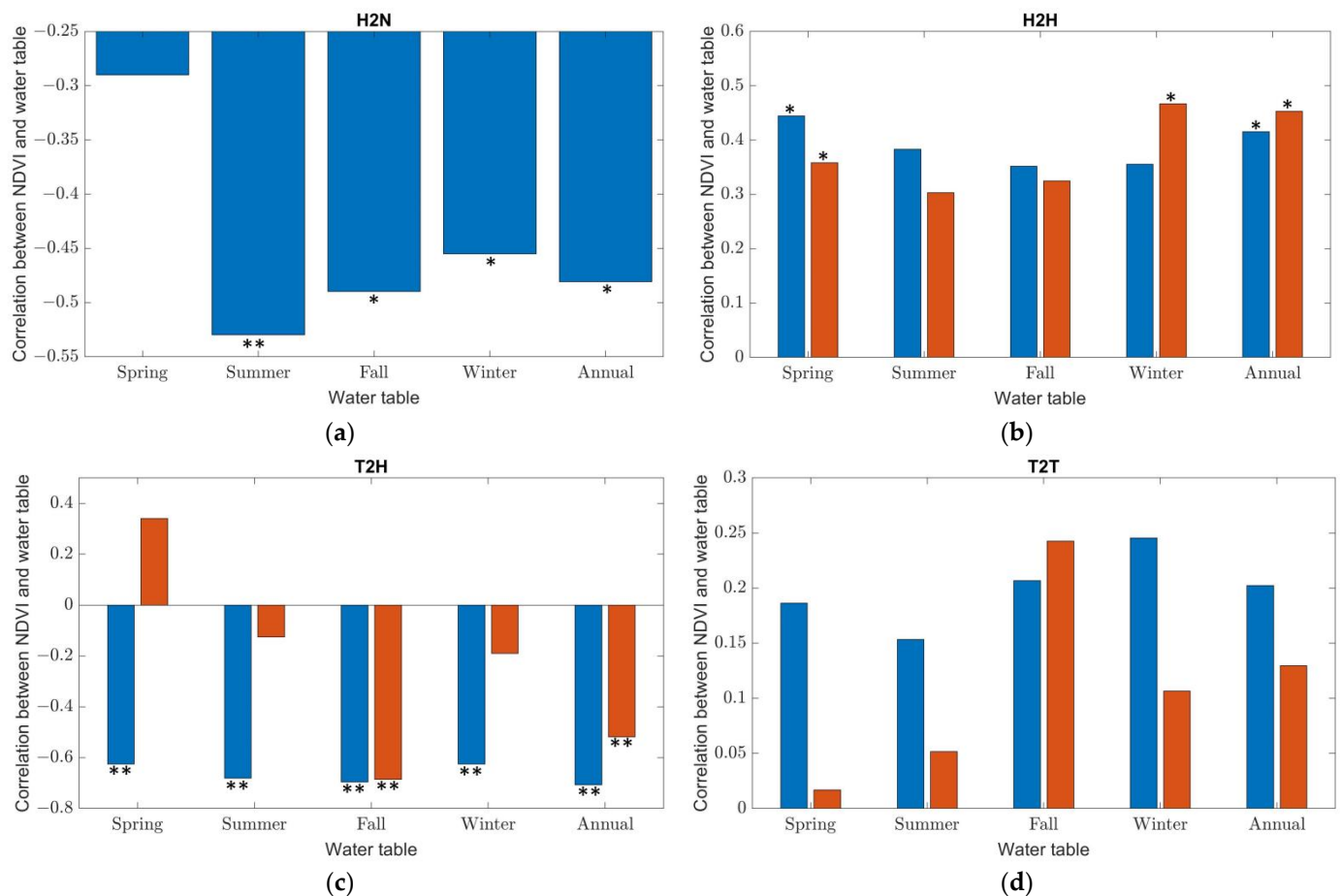


Figure 9. Cont.

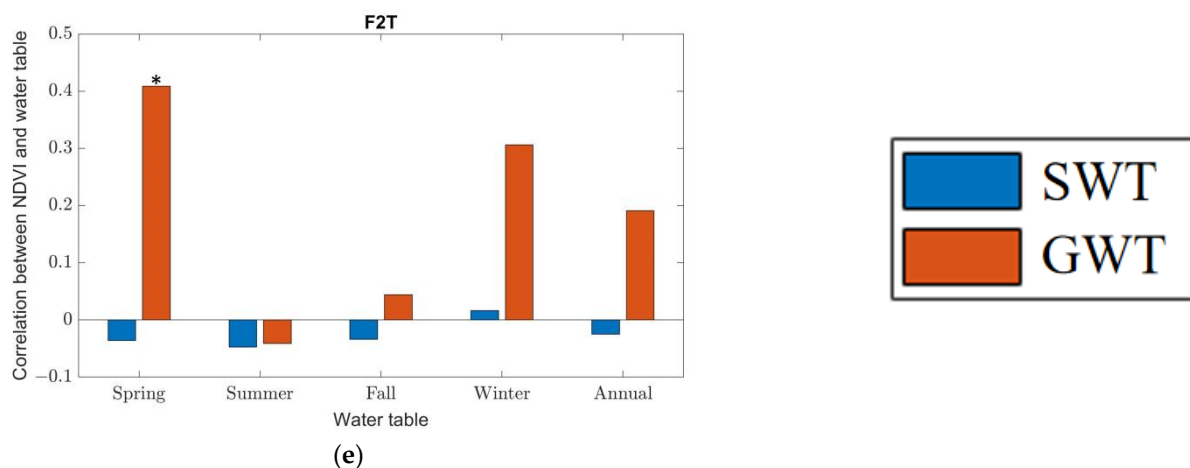


Figure 9. Correlations of grid-wise mean annual maximum NDVI to seasonal/annual mean saltwater tables (SWTs) and groundwater tables (GWTs) for different types of wetland evolution. (a) H2N: Emergent herbaceous wetlands degrading to non-vegetated areas (Type 6 degradation). Due to the fact that this triangular irregular grid was next to the sea (Figure 8a), and the simulated SWT was above the land surface, there was no distinction between saltwater and ground freshwater. Therefore, only the grid-wise mean annual maximum NDVI time series with seasonal/annual mean SWTs were presented; (b) H2H: Emergent herbaceous wetlands without degradation; (c) T2H: Transitional forested wetlands degrading to emergent herbaceous wetlands (Type 5 degradation); (d) T2T: Transitional forested wetlands without degradation; (e) F2T: Forested wetlands degrading to transitional forested wetlands (Type 3 degradation). $p < 0.05$ is denoted with a single star (*); $p < 0.01$ is denoted with double stars (**).

3.3.3. Thresholds of Water Table Depth to Coastal Wetland Degradation

We analyzed how summer GWTs and SWTs variations impact wetland degradation because summertime water tables (GWTs and SWTs) were most correlated with grid-wise mean annual maximum NDVI (Figure 9). Figure 10a shows the evolution of grid-wise mean annual maximum NDVI and summer SWTs for the pixels with the Type 6 degradation (i.e., emergent herbaceous wetlands degrading to non-vegetated areas). In 1995, the NDVI value was 0.18, suggesting that it was an emergent herbaceous wetland ($0.1 \leq \text{NDVI} < 0.4$). From 1995 to 2009, although the NDVI values of the wetland were occasionally below 0.1 due to environmental stresses/disturbances, its value came back to be higher than 0.1 a year later before 2010. Things changed in 2011. Its NDVI value fell from 0.13 to 0.06 in the year (2011) and never recovered by the end of the study period (2019), indicating that the emergent herbaceous wetlands degraded to non-vegetated areas (Type 6 degradation) in 2011. Correspondingly, the summertime SWT rose above ground by 0.16 m and maintained a high level after 2011. However, for emergent herbaceous wetlands without degradation, summertime SWTs and GWTs have never reached that height (Figure 10b). The results suggest that inundation negatively impacted the emergent herbaceous wetland, and 0.16 m above the ground might be a critical threshold of the water table for emergent herbaceous plants' survival.

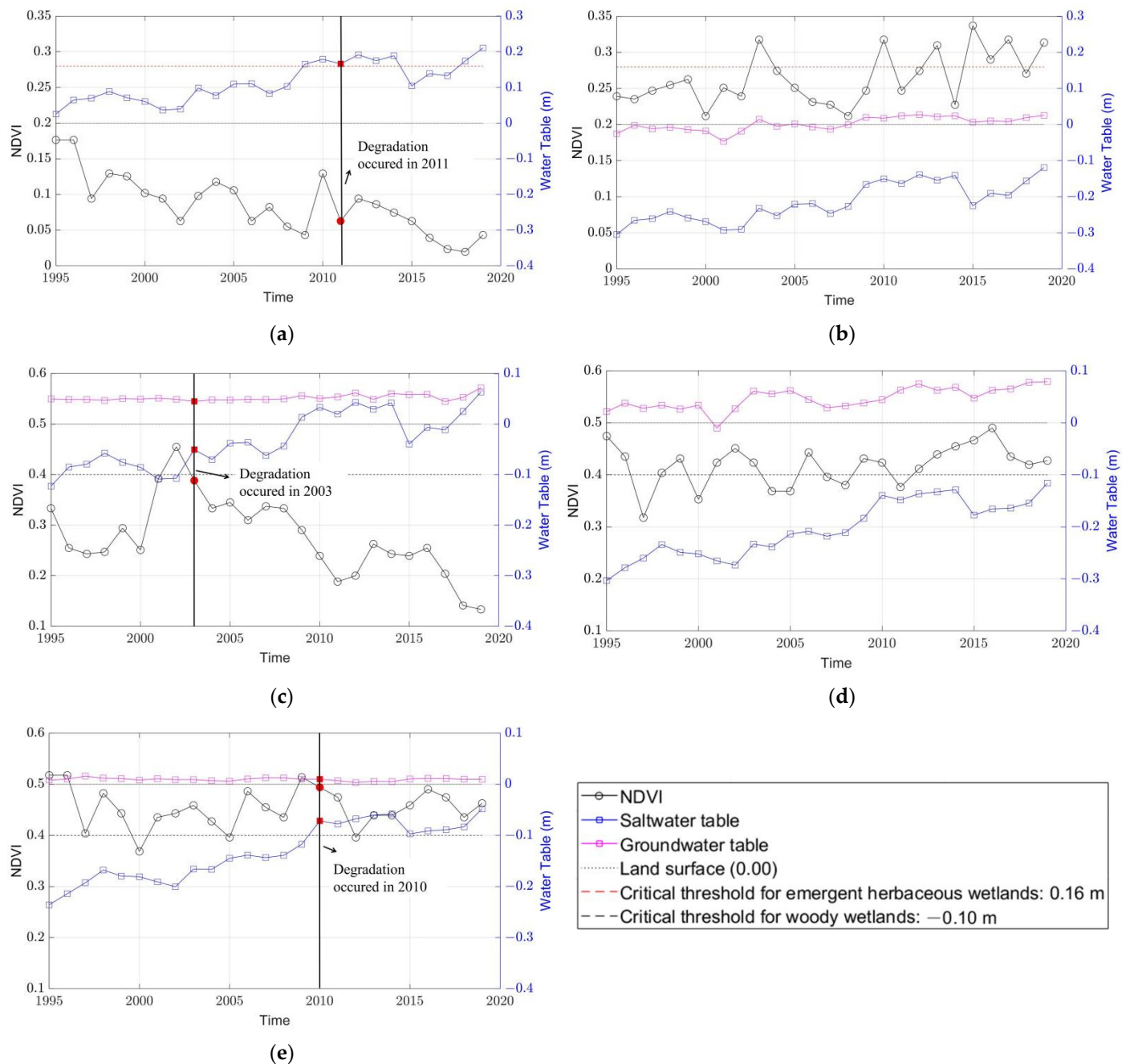


Figure 10. Evolution of the grid-wise mean annual maximum NDVI (left), summer GWTs (right, unit: m), and SWTs (right, unit: m) for (a) Type 6 degradation (emergent herbaceous wetlands degrading to non-vegetated areas). Summer mean GWTs are not presented for the same reason in Figure 9a; (b) Emergent herbaceous wetlands without degradation; (c) Type 5 degradation (transitional forested wetlands degrading to emergent herbaceous wetlands); (d) Transitional forested wetlands without degradation; (e) Type 3 degradation (forested wetlands degrading to transitional forested wetlands). Red and black horizontal dash lines represent the critical thresholds for emergent herbaceous wetlands (0.16 m) and woody wetlands (−0.10 m), respectively. Solid dots in red highlight NDVI, SWTs, and GWTs of degraded wetlands in the year degradation occurred.

For the pixels with the Type 5 degradation, forested wetlands transitioned to emergent herbaceous wetlands in 2003 (Figure 10c). The SWT dramatically rose from −0.11 m in 2002 to −0.05 m in 2003 and kept a high value greater than −0.10 m after that. Similar water table changes were also found for the Type 3 degradation in 2010 (Figure 10e); the SWT of the

wetlands was -0.12 m in 2009, then it jumped to -0.07 m in 2010, and never dropped back to lower than -0.10 m since 2010. Correspondingly, in 2010, forested wetlands degraded to transitional forested wetlands. In contrast, for the woody wetlands without degradation, the summertime SWT was lower than -0.10 m (Figure 10d). These results implied that the summertime SWT within 10 cm below the ground is critical for woody vegetation.

Figure 10 also provided insight into the opposite correlations between water tables and NDVI for degraded wetlands (Figure 9a,c,e) and non-degraded wetlands (Figure 9b,d). For the non-degraded emergent herbaceous wetlands (Figure 10b), during the 25 years, although the SWT had risen from -0.30 m in 1995 to -0.12 m in 2019 (Figure 10b), it still below the critical value (0.16 m). Meanwhile, rising GWTs allowed the plants to quickly draw fresh water from the soil, conducive to vegetation growth and increasing NDVI values [93]. Thus, positive correlations exist between water tables (GWTs and SWTs) and NDVI values in non-degraded wetlands (Figure 9b). On the contrary, for the degraded emergent herbaceous wetland (Figure 10a), the water table rose above the critical threshold (0.16 m), leading to the decline of vegetation (i.e., decreases of NDVI values). As a result, negative correlations between water tables and NDVI values can be found in the degraded wetlands (Figure 9a). Similar phenomena are observed in degraded (Figures 9c,e and 10c,e) and non-degraded woody wetlands (Figures 9d and 10d).

Coastal marshes have been widely considered salt-tolerant, while forests are salt-sensitive [20,52,94], which was also confirmed by our results. However, the thresholds of the water table for emergent herbaceous wetland and woody wetland survival are site-specific. These thresholds may change in other coastal wetland regions. As mentioned in Section 2.1, our study area is in a lagoonal environment with a micro-tidal inundation regime dominated by infrequent wind tides. Salinity in the sounds around the study area is controlled by the balance between the inflow of the Atlantic Ocean marine water through inlets along the Outer Banks and freshwater input from rivers, making this area an oligohaline condition [46,95–97]. Therefore, the ARNWR is distinct from other coastal wetlands due to its particular geomorphologic configuration. For a different wetland region with different hydraulic, vegetation, soil, climate, and geomorphologic settings, the PIHM-Wetland model could help to simulate the surface and subsurface hydrologic processes after modifying model parameters.

4. Conclusions

A new scheme is proposed to detect where and when coastal wetland degradation occurred on a regional scale by combining traditional remote sensing techniques and wetland hydrologic modeling. Applying the scheme to the ARNWR in NC, USA, we identified the spatio-temporal patterns of six types of coastal wetland degradation from 1995 to 2019 and determined critical thresholds of water tables for the degradation of different coastal wetland types.

Most of the coastal wetland degradation occurred within 2 km of the shoreline and in the past five years. During the 25-year study period, about 8.8% of the total wetlands have degraded, and 1.4% have been de-vegetated, mostly converted to open water. Although 380 ha of emergent herbaceous wetlands were converted into open water, the total area of emergent herbaceous wetlands increased by 213.0%, primarily due to a net loss of 1388 ha of woody wetlands.

The PIHM-Wetland model confirmed that both groundwater tables and saltwater tables were negatively (positively) correlated with NDVI within degraded (non-degraded) coastal wetlands. Rising sea levels and/or flooding inundated the emergent herbaceous wetlands on the shoreline, causing emergent herbaceous wetlands to degrade to non-vegetated areas. Elevated saltwater table posed stresses on inland forested wetlands and transitional forested wetlands, moving woody-herbaceous boundary further inland. In addition, we determined critical thresholds of water tables for the degradation of different coastal wetland types. Specifically, in the ARNWR, emergent herbaceous wetlands are likely to degrade when the water table is 0.16 m above the ground. In contrast, woody

plants are more sensitive to the rising of the saltwater table. When the saltwater tables are higher than -0.10 m, the forested and transitional wetlands are inclined to degrade.

This study establishes a remote sensing–hydrologic model integrated scheme for assessing coastal wetland health. Such a scheme offers an advanced tool in detecting and understanding coastal wetland degradation at a large scale and can be extended to other coastal wetland regions.

Supplementary Materials: The following supporting information can be downloaded at: <https://www.mdpi.com/article/10.3390/f13030411/s1>, Figure S1: Annual average sea levels observed at the local station Oregon Inlet Marina, NC from 1995 to 2019; Figure S2: Time series of NDVI of a randomly selected pixel with the Type 6 wetland degradation within ARNWR. Figure S3: Correlations of grid-wise mean seasonal NDVI to the seasonal saltwater table and groundwater table for different types of wetland evolution. Figure S4: Evolutions of the grid-wise mean seasonal NDVI, seasonal GWTs, and SWTs for degraded/non-degraded wetlands.

Author Contributions: Conceptualization, K.H. and W.L.; methodology, K.H., Y.Z. and W.L.; software, K.H. and Y.Z.; validation, K.H. and Y.Z.; formal analysis, K.H.; investigation, K.H.; resources, Y.Z. and W.L.; data curation, K.H. and Y.Z.; writing—original draft preparation, K.H.; writing—review and editing, K.H., Y.Z., W.L., G.S. and S.M.; visualization, K.H.; supervision, W.L. and G.S.; project administration, W.L.; funding acquisition, K.H. and W.L. All authors have read and agreed to the published version of the manuscript.

Funding: This research was funded by Duke Graduate Student Training Enhancement Grants (GSTEG) for Summer 2020 and Duke Nicholas School Dean’s Research Fund. The FIA DATA used in or as part of this publication were made possible, in part, by an Agreement from the United States Department of Agriculture’s Forest Service (USDA-FS). This publication may not necessarily express the views or opinions of the FS.

Data Availability Statement: NDVI images used in this study are openly available in <https://github.com/hkqcqq/CoastalWetlandDetection.git> (accessed on 12 February 2022). Groundwater table and saltwater table simulation outputs from the PIHM-Wetland model are available on request from the corresponding author due to that they are prohibitively large to store in a repository.

Acknowledgments: We thank Pan Chen for inspiring suggestions on developing the framework for detecting wetland degradation using NDVI time series.

Conflicts of Interest: The authors declare no conflict of interest.

References

1. Tockner, K.; Pusch, M.; Borchardt, D.; Lorang, M.S. Multiple stressors in coupled river-floodplain ecosystems. *Freshw. Biol.* **2010**, *55*, 135–151. [\[CrossRef\]](#)
2. Amlin, N.M.; Rood, S.B. Comparative tolerances of riparian willows and cottonwoods to water-table decline. *Wetlands* **2002**, *22*, 338–346. [\[CrossRef\]](#)
3. Conner, W.H.; Mihalia, I.; Wolfe, J. Tree community structure and changes from 1987 to 1999 in three Louisiana and three South Carolina forested wetlands. *Wetlands* **2002**, *22*, 58–70. [\[CrossRef\]](#)
4. Day, J.W.; Christian, R.R.; Boesch, D.M.; Yáñez-Arancibia, A.; Morris, J.; Twilley, R.R.; Naylor, L.; Schaffner, L.; Stevenson, C. Consequences of Climate Change on the Ecogeomorphology of Coastal Wetlands. *Estuar. Coast* **2008**, *31*, 477–491. [\[CrossRef\]](#)
5. Mitsch, W.J.; Gosselink, J.G. *Wetlands*, 5th ed.; John Wiley, Inc.: New York, NY, USA, 2015.
6. Rodríguez-Iturbe, I.; Porporato, A. *Ecohydrology of Water-Controlled Ecosystems: Soil Moisture and Plant Dynamics*; Cambridge University Press: New York, NY, USA, 2007.
7. Williams, K.; MacDonald, M.; Sternberg, L.D. Interactions of storm, drought, and sea-level rise on coastal forest: A case study. *J. Coast. Res.* **2003**, *19*, 1116–1121.
8. Winter, T.C. The vulnerability of wetlands to climate change: A hydrologic landscape perspective. *J. Am. Water Resour. Assoc.* **2000**, *36*, 305–311. [\[CrossRef\]](#)
9. Zhang, Y.; Li, W.; Sun, G.; King, J.S. Coastal wetland resilience to climate variability: A hydrologic perspective. *J. Hydrol.* **2019**, *568*, 275–284. [\[CrossRef\]](#)
10. Zhang, Y.; Li, W.; Sun, G.; Miao, G.; Noormets, A.; Emanuel, R.; King, J.S. Understanding coastal wetland hydrology with a new regional-scale, process-based hydrological model. *Hydrol. Process* **2018**, *32*, 3158–3173. [\[CrossRef\]](#)

11. Manzoni, S.; Maneas, G.; Scaini, A.; Psiloglou, B.E.; Destouni, G.; Lyon, S.W. Understanding coastal wetland conditions and futures by closing their hydrologic balance: The case of the Gialova lagoon, Greece. *Hydrol. Earth Syst. Sci.* **2020**, *24*, 3557–3571. [\[CrossRef\]](#)
12. Bianchette, T.A.; Liu, K.B.; Lam, N.N.; Kiage, L.M. Ecological impacts of Hurricane Ivan on the Gulf Coast of Alabama: A remote sensing study. *J. Coast. Res.* **2009**, *SI 56*, 1622–1626.
13. Hopfensperger, K.N.; Burgin, A.J.; Schoepfer, V.A.; Helton, A.M. Impacts of Saltwater Incursion on Plant Communities, Anaerobic Microbial Metabolism, and Resulting Relationships in a Restored Freshwater Wetland. *Ecosystems* **2014**, *17*, 792–807. [\[CrossRef\]](#)
14. Li, L.; Li, W.; Deng, Y. Summer rainfall variability over the Southeastern United States and its intensification in the 21st century as assessed by CMIP5 models. *J. Geophys. Res. Atmos.* **2013**, *118*, 340–354. [\[CrossRef\]](#)
15. Li, L.; Li, W.; Fu, R.; Deng, Y.; Wang, H. Changes to the North Atlantic Subtropical High and Its Role in the Intensification of Summer Rainfall Variability in the Southeastern United States. *J. Clim.* **2011**, *24*, 1499–1506. [\[CrossRef\]](#)
16. Wessels, K.J.; Van den Bergh, F.; Scholes, R.J. Limits to detectability of land degradation by trend analysis of vegetation index data. *Remote Sens. Environ.* **2012**, *125*, 10–22. [\[CrossRef\]](#)
17. Grenfell, M.C.; Ellery, W.N.; Garden, S.E.; Dini, J.; Van der Valk, A.G. The language of intervention: A review of concepts and terminology in wetland ecosystem repair. *Water SA* **2007**, *33*, 43–50. [\[CrossRef\]](#)
18. Shen, G.; Yang, X.; Jin, Y.; Xu, B.; Zhou, Q. Remote sensing and evaluation of the wetland ecological degradation process of the Zoige Plateau Wetland in China. *Ecol. Indic.* **2019**, *104*, 48–58. [\[CrossRef\]](#)
19. Smart, L.S.; Taillie, P.J.; Poulter, B.; Vukomanovic, J.; Singh, K.K.; Swenson, J.J.; Mitsova, H.; Smith, J.W.; Meentemeyer, R.K. Aboveground carbon loss associated with the spread of ghost forests as sea levels rise. *Environ. Res. Lett.* **2020**, *15*, 104028. [\[CrossRef\]](#)
20. Kirwan, M.L.; Gedan, K.B. Sea-level driven land conversion and the formation of ghost forests. *Nat. Clim. Chang.* **2019**, *9*, 450–457. [\[CrossRef\]](#)
21. Cui, L.; Li, G.; Ouyang, N.; Mu, F.; Yan, F.; Zhang, Y.; Huang, X. Analyzing Coastal Wetland Degradation and its Key Restoration Technologies in the Coastal Area of Jiangsu, China. *Wetlands* **2018**, *38*, 525–537. [\[CrossRef\]](#)
22. Qiu, Z.; Luo, L.; Mao, D.; Du, B.; Feng, K.; Jia, M.; Wang, Z. Using Multisource Geospatial Data to Identify Potential Wetland Rehabilitation Areas: A Pilot Study in China's Sanjiang Plain. *Water* **2020**, *12*, 2496. [\[CrossRef\]](#)
23. Shi, S.; Chang, Y.; Wang, G.; Li, Z.; Hu, Y.; Liu, M.; Li, Y.; Li, B.; Zong, M.; Huang, W. Planning for the wetland restoration potential based on the viability of the seed bank and the land-use change trajectory in the Sanjiang Plain of China. *Sci. Total Environ.* **2020**, *733*, 139208. [\[CrossRef\]](#) [\[PubMed\]](#)
24. Huo, L.; Chen, Z.; Zou, Y.; Lu, X.; Guo, J.; Tang, X. Effect of Zoige alpine wetland degradation on the density and fractions of soil organic carbon. *Ecol. Eng.* **2013**, *51*, 287–295. [\[CrossRef\]](#)
25. Loughheed, V.L.; McIntosh, M.D.; Parker, C.A.; Stevenson, R.J. Wetland degradation leads to homogenization of the biota at local and landscape scales. *Freshw. Biol.* **2008**, *53*, 2402–2413. [\[CrossRef\]](#)
26. Malekmohammadi, B.; Rahimi Blouchi, L. Ecological risk assessment of wetland ecosystems using Multi Criteria Decision Making and Geographic Information System. *Ecol. Indic.* **2014**, *41*, 133–144. [\[CrossRef\]](#)
27. Rodríguez, C.F.; Bécares, E.; Fernández-Aláez, M.; Fernández-Aláez, C. Loss of diversity and degradation of wetlands as a result of introducing exotic crayfish. *Biol. Invasions* **2005**, *7*, 75–85. [\[CrossRef\]](#)
28. Brooks, R.P.; Wardrop, D.H.; Cole, C.A.; Campbell, D.A. Are we purveyors of wetland homogeneity?: A model of degradation and restoration to improve wetland mitigation performance. *Ecol. Eng.* **2005**, *24*, 331–340. [\[CrossRef\]](#)
29. Keim, R.F.; Chambers, J.L.; Hughes, M.S.; Nyman, J.A.; Miller, C.A.; Amos, B.J.; Conner, W.H.; Day, J.W.; Faulkner, S.P.; Gardiner, E.S.; et al. Ecological consequences of changing hydrological conditions in wetland forests of coastal Louisiana. In *Coastal Environment and Water Quality*; Xu, Y.J., Singh, V.P., Eds.; 6 Water Resources Publications, LLC: Highlands Ranch, CO, USA, 2006; pp. 383–396.
30. Aguilos, M.; Mitra, B.; Noormets, A.; Minick, K.; Prajapati, P.; Gavazzi, M.; Sun, G.; McNulty, S.; Li, X.; Domec, J.-C.; et al. Long-term carbon flux and balance in managed and natural coastal forested wetlands of the Southeastern USA. *Agric. For. Meteorol.* **2020**, *288*, 108022. [\[CrossRef\]](#)
31. Uzarski, D.G.; Brady, V.J.; Cooper, M.J.; Wilcox, D.A.; Albert, D.A.; Axler, R.P.; Bostwick, P.; Brown, T.N.; Ciborowski, J.J.H.; Danz, N.P.; et al. Standardized Measures of Coastal Wetland Condition: Implementation at a Laurentian Great Lakes Basin-Wide Scale. *Wetlands* **2017**, *37*, 15–32. [\[CrossRef\]](#)
32. Doyle, C.; Beach, T.; Luzzadder-Beach, S. Tropical Forest and Wetland Losses and the Role of Protected Areas in Northwestern Belize, Revealed from Landsat and Machine Learning. *Remote Sens.* **2021**, *13*, 379. [\[CrossRef\]](#)
33. Ury, E.A.; Yang, X.; Wright, J.P.; Bernhardt, E.S. Rapid deforestation of a coastal landscape driven by sea-level rise and extreme events. *Ecol. Appl.* **2021**, *31*, e02339. [\[CrossRef\]](#)
34. Guo, M.; Li, J.; Sheng, C.; Xu, J.; Wu, L. A Review of Wetland Remote Sensing. *Sensors* **2017**, *17*, 777. [\[CrossRef\]](#) [\[PubMed\]](#)
35. Jin, H.; Huang, C.; Lang, M.W.; Yeo, I.-Y.; Stehman, S.V. Monitoring of wetland inundation dynamics in the Delmarva Peninsula using Landsat time-series imagery from 1985 to 2011. *Remote Sens. Environ.* **2017**, *190*, 26–41. [\[CrossRef\]](#)
36. Klemas, V. Remote sensing techniques for studying coastal ecosystems: An overview. *J. Coast. Res.* **2011**, *27*, 2–17.
37. Jiang, Z.; Huete, A.R.; Chen, J.; Chen, Y.; Li, J.; Yan, G.; Zhang, X. Analysis of NDVI and scaled difference vegetation index retrievals of vegetation fraction. *Remote Sens. Environ.* **2006**, *101*, 366–378. [\[CrossRef\]](#)

38. Lambert, J.; Denux, J.-P.; Verbesselt, J.; Balent, G.; Cheret, V. Detecting Clear-Cuts and Decreases in Forest Vitality Using MODIS NDVI Time Series. *Remote Sens.* **2015**, *7*, 3588–3612. [\[CrossRef\]](#)
39. Klemas, V. Remote sensing of emergent and submerged wetlands: An overview. *Int. J. Remote Sens.* **2013**, *34*, 6286–6320. [\[CrossRef\]](#)
40. Yuan, J.; Cohen, M.J. Remote detection of ecosystem degradation in the Everglades ridge-slough landscape. *Remote Sens. Environ.* **2020**, *247*, 111917. [\[CrossRef\]](#)
41. Bai, Z.G.; Dent, D.L.; Olsson, L.; Schaepman, M.E. Proxy global assessment of land degradation. *Soil Use Manag.* **2008**, *24*, 223–234. [\[CrossRef\]](#)
42. Colwell, J.E. Vegetation canopy reflectance. *Remote Sens. Environ.* **1974**, *3*, 175–183. [\[CrossRef\]](#)
43. Huete, A.R.; Liu, H.Q.; Batchily, K.V.; Van Leeuwen, W.J. A comparison of vegetation indices over a global set of TM images for EOS-MODIS. *Remote Sens. Environ.* **1997**, *59*, 440–451. [\[CrossRef\]](#)
44. Pereira, O.; Ferreira, L.; Pinto, F.; Baumgarten, L. Assessing Pasture Degradation in the Brazilian Cerrado Based on the Analysis of MODIS NDVI Time-Series. *Remote Sens.* **2018**, *10*, 1761. [\[CrossRef\]](#)
45. Eckert, S.; Hüsler, F.; Liniger, H.; Hodel, E. Trend analysis of MODIS NDVI time series for detecting land degradation and regeneration in Mongolia. *J. Arid Environ.* **2015**, *113*, 16–28. [\[CrossRef\]](#)
46. Moorhead, K.K.; Brinson, M.M. Response of wetlands to rising sea level in the lower coastal plain of North Carolina. *Ecol. Appl.* **1995**, *5*, 261–271. [\[CrossRef\]](#)
47. Moorhead, K.K.; Cook, A.E. A comparison of hydric soils, wetlands, and land use in coastal North Carolina. *Wetlands* **1992**, *12*, 99–105. [\[CrossRef\]](#)
48. Poulter, B. Interactions between Landscape Disturbance and Gradual Environmental Change: Plant Community Migration in Response to Fire and Sea Level Rise. Ph.D. Thesis, Duke University, Durham, NC, USA, 2005.
49. Taillie, P.J.; Moorman, C.E.; Poulter, B.; Ardón, M.; Emanuel, R.E. Decadal-Scale Vegetation Change Driven by Salinity at Leading Edge of Rising Sea Level. *Ecosystems* **2019**, *22*, 1918–1930. [\[CrossRef\]](#)
50. Aguilos, M.; Sun, G.; Noormets, A.; Domec, J.C.; McNulty, S.; Gavazzi, M.; Prajapati, P.; Minick, K.J.; Mitra, B.; King, J. Ecosystem productivity and evapotranspiration are tightly coupled in Loblolly Pine (*Pinus taeda* L.) plantations along the coastal plain of the southeastern US. *Forests* **2021**, *12*, 1123. [\[CrossRef\]](#)
51. Miao, G.; Noormets, A.; Domec, J.C.; Trettin, C.C.; McNulty, S.G.; Sun, G.; King, J.S. The effect of water table fluctuation on soil respiration in a lower coastal plain forested wetland in the southeastern US. *J. Geophys. Res.-Biogeosci.* **2013**, *118*, 1748–1762. [\[CrossRef\]](#)
52. Schieder, N.W.; Walters, D.C.; Kirwan, M.L. Massive Upland to Wetland Conversion Compensated for Historical Marsh Loss in Chesapeake Bay, USA. *Estuar. Coast* **2018**, *41*, 940–951. [\[CrossRef\]](#)
53. Walker, J.S.; Kopp, R.E.; Shaw, T.A.; Cahill, N.; Khan, N.S.; Barber, D.C.; Ashe, E.L.; Brain, M.J.; Clear, J.L.; Corbett, D.R.; et al. Common Era sea-level budgets along the U.S. Atlantic coast. *Nat. Commun.* **2021**, *12*, 1841. [\[CrossRef\]](#)
54. Hunter, R.G.; Day, J.W.; Lane, R.R.; Shaffer, G.P.; Day, J.N.; Conner, W.H.; Rybczyk, J.M.; Mistich, J.A.; Ko, J.Y. Using natural wetlands for municipal effluent assimilation: A half-century of experience for the Mississippi River Delta and surrounding environs. In *Multifunctional Wetlands*; Nagabhatla, N., Metcalfe, C.D., Eds.; Springer Nature: Cham, Switzerland, 2018; pp. 15–81.
55. Lang, M.; Stedman, S.-M.; Nettles, J.; Griffin, R. Coastal Watershed Forested Wetland Change and Opportunities for Enhanced Collaboration with the Forestry Community. *Wetlands* **2020**, *40*, 7–19. [\[CrossRef\]](#)
56. Richardson, C.J. Pocosins: An ecological perspective. *Wetlands* **1991**, *11*, 335–354. [\[CrossRef\]](#)
57. Kennedy, R.E.; Andréfouët, S.; Cohen, W.B.; Gómez, C.; Griffiths, P.; Hais, M.; Healey, S.P.; Helmer, E.H.; Hostert, P.; Lyons, M.B.; et al. Bringing an ecological view of change to Landsat-based remote sensing. *Front. Ecol. Environ.* **2014**, *12*, 339–346. [\[CrossRef\]](#)
58. Wulder, M.A.; Masek, J.G.; Cohen, W.B.; Loveland, T.R.; Woodcock, C.E. Opening the archive: How free data has enabled the science and monitoring promise of Landsat. *Remote Sens. Environ.* **2012**, *122*, 2–10. [\[CrossRef\]](#)
59. Eidenshink, J. The 1990 conterminous U. S. AVHRR data set. *Photogramm. Eng. Remote Sens.* **1992**, *58*, 809–813.
60. Gamon, J.A.; Field, C.B.; Goulden, M.L.; Griffin, K.L.; Hartley, A.E.; Joel, G.; Penuelas, J.; Valentini, R. Relationships between NDVI, canopy structure, and photosynthesis in three Californian vegetation types. *Ecol. Appl.* **1995**, *5*, 28–41. [\[CrossRef\]](#)
61. Sun, C.; Liu, Y.; Zhao, S.; Zhou, M.; Yang, Y.; Li, F. Classification mapping and species identification of salt marshes based on a short-time interval NDVI time-series from HJ-1 optical imagery. *Int. J. Appl. Earth Obs.* **2016**, *45*, 27–41. [\[CrossRef\]](#)
62. Zhang, X.; Wu, S.; Yan, X.; Chen, Z. A global classification of vegetation based on NDVI, rainfall and temperature. *Int. J. Climatol.* **2017**, *37*, 2318–2324. [\[CrossRef\]](#)
63. Jamali, S.; Seaquist, J.; Eklundh, L.; Ardö, J. Automated mapping of vegetation trends with polynomials using NDVI imagery over the Sahel. *Remote Sens. Environ.* **2014**, *141*, 79–89. [\[CrossRef\]](#)
64. Karlsen, S.; Elvebakk, A.; Høgda, K.; Grydeland, T. Spatial and Temporal Variability in the Onset of the Growing Season on Svalbard, Arctic Norway—Measured by MODIS-NDVI Satellite Data. *Remote Sens.* **2014**, *6*, 8088–8106. [\[CrossRef\]](#)
65. Anyamba, A.; Tucker, C.J. Analysis of Sahelian vegetation dynamics using NOAA-AVHRR NDVI data from 1981–2003. *J. Arid Environ.* **2005**, *63*, 596–614. [\[CrossRef\]](#)
66. Zheng, Y.; Han, J.; Huang, Y.; Fassnacht, S.R.; Xie, S.; Lv, E.; Chen, M. Vegetation response to climate conditions based on NDVI simulations using stepwise cluster analysis for the Three-River Headwaters region of China. *Ecol. Indic.* **2018**, *92*, 18–29. [\[CrossRef\]](#)

67. Bhandari, A.K.; Kumar, A.; Singh, G.K. Feature Extraction using Normalized Difference Vegetation Index (NDVI): A Case Study of Jabalpur City. *Proc. Technol.* **2012**, *6*, 612–621. [\[CrossRef\]](#)
68. Chouhan, A.P.S.; Sarma, A.K. Modern heterogeneous catalysts for biodiesel production: A comprehensive review. *Renew. Sustain. Energy Rev.* **2011**, *15*, 4378–4399. [\[CrossRef\]](#)
69. Gandhi, G.M.; Parthiban, S.; Thummalu, N.; Christy, A. Ndvi: Vegetation Change Detection Using Remote Sensing and Gis—A Case Study of Vellore District. *Procedia Comput. Sci.* **2015**, *57*, 1199–1210. [\[CrossRef\]](#)
70. Meneses-Tovar, C.L. NDVI as indicator of degradation. *Unasylva* **2011**, *62*, 39–46.
71. Roustai, I.; Olafsson, H.; Moniruzzaman, M.; Ardö, J.; Zhang, H.; Mushore, T.D.; Shahin, S.; Azim, S. The 2000–2017 drought risk assessment of the western and southwestern basins in Iran. *Model. Earth Syst. Environ.* **2020**, *6*, 1201–1221. [\[CrossRef\]](#)
72. Weier, J.; Herring, D. *Measuring Vegetation (NDVI & EVI)*; NASA Earth Observatory: Washington, DC, USA, 2000.
73. Bechtold, W.A.; Patterson, P.L. (Eds.) *The Enhanced Forest Inventory and Analysis Program-National Sampling Design and Estimation Procedures. Gen. Technol. Rep. SRS-80*; U.S. Department of Agriculture, Forest Service, Southern Research Station: Asheville, NC, USA, 2005; p. 85.
74. Burrill, E.A.; DiTommaso, A.M.; Turner, J.A.; Pugh, S.A.; Menlove, J.; Christiansen, G.; Perry, C.J.; Conkling, B.L. The Forest Inventory and Analysis Database: Database Description and User Guide Version 9.0.1 for Phase 2. U.S. Department of Agriculture, Forest Service. 1026p. Available online: <http://www.fia.fs.fed.us/library/database-documentation/> (accessed on 21 September 2020).
75. C-CAP Regional Land Cover and Change. NOAA. Available online: www.coast.noaa.gov/htdata/raster1/landcover/bulkdownload/30m_lc/ (accessed on 20 July 2021).
76. Xia, Y.; Mitchell, K.; Ek, M.; Sheffield, J.; Cosgrove, B.; Wood, E.; Luo, L.; Alonge, C.; Wei, H.; Meng, J.; et al. Continental-scale water and energy flux analysis and validation for the North American Land Data Assimilation System project phase 2 (NLDAS-2): 1. Intercomparison and application of model products. *J. Geophys. Res. Atmos.* **2012**, *117*, D03109. [\[CrossRef\]](#)
77. Nash, J.E.; Sutcliffe, J.V. River flow forecasting through conceptual models part I—A discussion of principles. *J. Hydrol.* **1970**, *10*, 282–290. [\[CrossRef\]](#)
78. Liu, Y.; Kumar, M. Role of meteorological controls on interannual variations in wet-period characteristics of wetlands. *Water Resour. Res.* **2016**, *52*, 5056–5074. [\[CrossRef\]](#)
79. Todd, M.J.; Muneeppeerakul, R.; Pumo, D.; Azale, S.; Miralles-Wilhelm, F.; Rinaldo, A.; Rodriguez-Iturbe, I. Hydrological drivers of wetland vegetation community distribution within Everglades National Park, Florida. *Adv. Water Resour.* **2010**, *33*, 1279–1289. [\[CrossRef\]](#)
80. Wei, J.; Huang, W.; Li, Z.; Sun, L.; Zhu, X.; Yuan, Q.; Liu, L.; Cribb, M. Cloud detection for Landsat imagery by combining the random forest and superpixels extracted via energy-driven sampling segmentation approaches. *Remote Sens. Environ.* **2020**, *248*, 112005. [\[CrossRef\]](#)
81. Zhu, Z.; Qiu, S.; He, B.; Deng, C. Cloud and cloud shadow detection for Landsat images: The fundamental basis for analyzing Landsat time series. In *Remote Sensing Time Series Image Processing*; Weng, Q., Ed.; CRC Press: Boca Raton, FL, USA, 2018; pp. 3–23.
82. Armitage, A.R.; Weaver, C.A.; Kominoski, J.S.; Pennings, S.C. Resistance to Hurricane Effects Varies Among Wetland Vegetation Types in the Marsh–Mangrove Ecotone. *Estuar. Coast* **2020**, *43*, 960–970. [\[CrossRef\]](#)
83. Hu, T.; Smith, R. The Impact of Hurricane Maria on the Vegetation of Dominica and Puerto Rico Using Multispectral Remote Sensing. *Remote Sens.* **2018**, *10*, 827. [\[CrossRef\]](#)
84. Steyer, G.D.; Couvillion, B.R.; Barras, J.A. Monitoring Vegetation Response to Episodic Disturbance Events by using Multitemporal Vegetation Indices. *J. Coast. Res.* **2013**, *63*, 118–130. [\[CrossRef\]](#)
85. Ke, Y.; Im, J.; Lee, J.; Gong, H.; Ryu, Y. Characteristics of Landsat 8 OLI-derived NDVI by comparison with multiple satellite sensors and in-situ observations. *Remote Sens. Environ.* **2015**, *164*, 298–313. [\[CrossRef\]](#)
86. Roy, D.P.; Kovalskyy, V.; Zhang, H.K.; Vermote, E.F.; Yan, L.; Kumar, S.S.; Egorov, A. Characterization of Landsat-7 to Landsat-8 reflective wavelength and normalized difference vegetation index continuity. *Remote Sens. Environ.* **2016**, *185*, 57–70. [\[CrossRef\]](#)
87. Xu, D.; Guo, X. Compare NDVI Extracted from Landsat 8 Imagery with that from Landsat 7 Imagery. *Am. J. Remote Sens.* **2014**, *2*, 10–14. [\[CrossRef\]](#)
88. Cairns, J., Jr. Setting ecological restoration goals for technical feasibility and scientific validity. *Ecol. Eng.* **2000**, *15*, 171–180. [\[CrossRef\]](#)
89. Kentula, M.E. Perspectives on setting success criteria for wetland restoration. *Ecol. Eng.* **2000**, *15*, 199–209. [\[CrossRef\]](#)
90. Broadfoot, W.M.; Williston, H.L. Flooding effects on southern forests. *J. For.* **1973**, *71*, 584–587.
91. Copini, P.; Den Ouden, J.; Robert, E.M.; Tardif, J.C.; Loesberg, W.A.; Goudzwaard, L.; Sass-Klaassen, U. Flood-ring formation and root development in response to experimental flooding of young *Quercus robur* trees. *Front. Plant Sci.* **2016**, *7*, 775. [\[CrossRef\]](#) [\[PubMed\]](#)
92. Siebel, H.N.; Blom, C.W. Effects of irregular flooding on the establishment of tree species. *Acta Bot. Neerl.* **1998**, *47*, 231–240.
93. Xu, H.; Ye, M.; Li, J.-M. Changes in groundwater levels and the response of natural vegetation to transfer of water to the lower reaches of the Tarim River. *J. Environ. Sci.* **2007**, *19*, 1199–1207. [\[CrossRef\]](#)
94. Kirwan, M.L.; Kirwan, J.L.; Copenheaver, C.A. Dynamics of an Estuarine Forest and its Response to Rising Sea Level. *J. Coast. Res.* **2007**, *232*, 457–463. [\[CrossRef\]](#)

-
95. Costa, C.S.; Marangoni, J.C.; Azevedo, A.M. Plant zonation in irregularly flooded salt marshes: Relative importance of stress tolerance and biological interactions. *J. Ecol.* **2003**, *91*, 951–965. [[CrossRef](#)]
 96. Kemp, A.C.; Horton, B.P.; Culver, S.J. Distribution of modern salt-marsh foraminifera in the Albemarle–Pamlico estuarine system of North Carolina, USA: Implications for sea-level research. *Mar. Micropaleontol.* **2009**, *72*, 222–238. [[CrossRef](#)]
 97. Poulter, B.; Christensen, N.L.; Qian, S.S. Tolerance of *Pinus taeda* and *Pinus serotina* to low salinity and flooding: Implications for equilibrium vegetation dynamics. *J. Veg. Sci.* **2008**, *19*, 15–22. [[CrossRef](#)]